



# Early summer hydroclimatic signals are captured well by tree-ring earlywood width in the eastern Qinling Mountains, central China

Yesi Zhao<sup>1,2</sup>, Jiangfeng Shi<sup>1,3</sup>, Shiyuan Shi<sup>1</sup>, Xiaoqi Ma<sup>1</sup>, Weijie Zhang<sup>1</sup>, Bowen Wang<sup>1</sup>, Xuguang Sun<sup>4</sup>, Huayu Lu<sup>1</sup>, and Achim Bräuning<sup>2</sup>

<sup>1</sup>School of Geography and Ocean Science, Nanjing University, Nanjing 210023, China

<sup>2</sup>Institute of Geography, Friedrich-Alexander-Universität Erlangen-Nürnberg, Erlangen 91058, Germany

<sup>3</sup>Laboratory of Tree-Ring Research, University of Arizona, Tucson 85721, USA

<sup>4</sup>School of Atmospheric Sciences, Nanjing University, Nanjing 210023, China

**Correspondence:** Jiangfeng Shi (shijf@nju.edu.cn)

Received: 21 October 2018 – Discussion started: 29 October 2018

Revised: 30 May 2019 – Accepted: 4 June 2019 – Published: 25 June 2019

**Abstract.** In the humid and semi-humid regions of China, tree-ring-width (TRW) chronologies offer limited moisture-related climatic information. To gather additional climatic information, it would be interesting to explore the potential of the intra-annual tree-ring-width indices (i.e., the earlywood width, EWW, and latewood width, LWW). To achieve this purpose, TRW, EWW, and LWW were measured from the tree-ring samples of *Pinus tabulaeformis* originating from the semi-humid eastern Qinling Mountains, central China. Standard (STD) and signal-free (SSF) chronologies of all parameters were created using these detrending methods including (1) negative exponential functions combined with linear regression with negative (or zero) slope (NELR), (2) cubic smoothing splines with a 50 % frequency cutoff at 67 % of the series length (SP67), and (3) age-dependent splines with an initial stiffness of 50 years (SPA50). The results showed that EWW chronologies were significantly negatively correlated with temperature but positively correlated with precipitation and soil moisture conditions during the current early-growing season. By contrast, LWW and TRW chronologies had weaker relationships with these climatic factors. The strongest climatic signal was detected for the EWW STD chronology detrended with the NELR method, explaining 50 % of the variance in the May–July self-calibrated Palmer Drought Severity Index (MJJ scPDSI) during the instrumental period 1953–2005. Based on this relationship, the MJJ scPDSI was reconstructed back to 1868 using a linear regression function. The reconstruction was validated by compar-

ison with other hydroclimatic reconstructions and historical document records from adjacent regions. Our results highlight the potential of intra-annual tree-ring indices for reconstructing seasonal hydroclimatic variations in humid and semi-humid regions of China. Furthermore, our reconstruction exhibits a strong in-phase relationship with a newly proposed East Asian summer monsoon index (EASMI) before the 1940s on the decadal and longer timescales, which may be due to the positive response of the local precipitation to EASMI. Nonetheless, the cause for the weakened relationship after the 1940s is complex, and cannot be solely attributed to the changing impacts of precipitation and temperature.

## 1 Introduction

Most of the existing hydroclimatic reconstructions based on tree-ring width (TRW) in China were conducted for the regions located between the 200 and 600 mm annual precipitation isolines (Y. Liu et al., 2018), close to the northern fringe of the Asian summer monsoon realm. Nonetheless, there exists still a small number of hydroclimate reconstructions in the core monsoon region, e.g., from southeastern China (e.g., Cai et al., 2017; Chen et al., 2016a; Shi et al., 2015), northern China (e.g., Chen et al., 2016b; Hughes et al., 1994; Lei et al., 2014; Liu et al., 2002), and from the Hengduan Mountains in southwestern China (e.g., Fan et al., 2008;

Fang et al., 2010b; Gou et al., 2013; Li et al., 2017). Since precipitation is spatially highly variable (Ding et al., 2013), hydroclimatic variations close to the monsoon boundary cannot completely represent those in the core monsoon region (Y. Liu et al., 2018). Thus, additional hydroclimatic reconstructions are needed from the center of the monsoon region.

Some TRW chronologies within the monsoon region showed weak or unstable hydroclimatic signals (e.g., Li et al., 2016; Shi et al., 2012; Wang et al., 2018), making them unsuitable to derive reliable reconstructions. By contrast, intra-annually resolved tree-ring width (i.e., earlywood width, EWW, and latewood width, LWW) provided stronger hydroclimatic signals than TRW in some cases (Chen et al., 2012; Zhao et al., 2017a). This might be because the movement of the monsoon rain belt can lead to an uneven distribution of precipitation during the growing season (Jiang et al., 2006), thus causing restrictions to water availability during parts of the growing season, and limiting the growth of certain intra-ring sectors rather than the total ring width (X. Liu et al., 2018). EWW and LWW have been successfully applied for reconstructing long-term variations in seasonal rainfall (Hansen et al., 2017), drought (standardized precipitation evapotranspiration index (SPEI); Zhao et al., 2017b), and streamflow (Guan et al., 2018) in the monsoon region.

The eastern Qinling Mountains are located within the core region of the East Asian summer monsoon (EASM) and are characterized by a transitional climate, from a warm temperate to subtropical climate. In this region, Shi et al. (2012) built four TRW chronologies of *Pinus tabulaeformis* along an elevation gradient from 1200 to 1950 m above sea level (a.s.l.). The TRW chronologies of the two low-altitude sites, i.e., Baiyunshan and Longchiman, exhibited a positive response to precipitation and negative response to temperature during early summer, showing a sign of water stress. However, the dendroclimatic potential of EWW and LWW were not explored.

Meanwhile, tree growth at an adjacent site was found to be more restricted by the drought index, represented by the well-known PDSI (Palmer Drought Severity Index), rather than by precipitation or temperature (Peng et al., 2014). Briefly, the PDSI monitors the cumulative departure of surface water balance in terms of the difference between the amount of precipitation required to retain a normal water-balance level and the amount of actual precipitation (Palmer, 1965; Wells et al., 2004). In addition, the SPEI, a drought index representing water balance in the form of difference between precipitation and potential evapotranspiration (Vicente-Serrano et al., 2010), was reported to constrain latewood growth at a well-drained site in the core region of EASM (Zhao et al., 2017a, b). According to these findings, complex drought indices like the PDSI and SPEI should also be incorporated into the climate–tree-growth relationship assessment of tree-ring variables.

Recently, a new East Asian summer monsoon index (EASMI) based on the 200 hPa zonal wind anomalies was

proposed by Zhao et al. (2015). The new EASMI performs better in describing precipitation and temperature variations over East Asia than existing indices. Suppose a strong EASM occurred, the new EASMI would indicate abundant precipitation and relatively low temperature over the core region of EASM, particularly around the area of the Meiyu/Changma/Baiu rainband (27.5–32.5° N, 105–120° E and 30–37.5° N, 127.5–150° E; Fig. 1a), which is the center of the leading mode of EASM precipitation (Wang et al., 2008; Zhao et al., 2015). It would be interesting to study the response of local hydroclimate to EASM from a long-term perspective in combination with these tree-ring materials and the new EASMI.

Considering the TRW series of *P. tabulaeformis* in Baiyunshan and Longchiman are mainly restricted by the early summer moisture conditions, we hypothesize that the early summer hydroclimatic signals might be strengthened only using EWW, since earlywood is mostly formed before mid-July (Zhang et al., 1982). Therefore, the objectives of this study are (1) to verify that EWW is more sensitive to early summer hydroclimatic factors than TRW and LWW for *P. tabulaeformis* at Baiyunshan and Longchiman, (2) to reconstruct early summer hydroclimate variations using EWW, and (3) to tentatively explore the relationship between the reconstructed hydroclimate variability and EASMI.

## 2 Materials and methods

### 2.1 Study sites

In this study, the dated tree-ring samples of *P. tabulaeformis* are those presented by Shi et al. (2012). Briefly, they were collected from two sampling sites on Mount Funiu in 2006 and 2008 separately: Baiyunshan (33.63° N, 111.85° E) and Longchiman (33.68° N, 112.05° E; Fig. 1b). The sampling sites are located on mountain tops, where soils are thin and well drained. The elevations of Baiyunshan and Longchiman range from 1200 to 1300 m a.s.l. and from 1340 to 1400 m a.s.l., respectively. The regional annual mean temperature and annual total precipitation are 14.1 °C and 809.1 mm, respectively. Most of the annual total precipitation drops in the warm season (Fig. 2). More detailed information on the study sites can be found in Shi et al. (2012).

### 2.2 Tree-ring data

*P. tabulaeformis* is a widely distributed conifer species in northern China with the extension from 31°00' N to 43°33' N, and 103°20' E to 124°45' E (Xu et al., 1981). By studying the cambial dynamics of *P. tabulaeformis* in its northern distribution limit (43°14.11' N, 116°23.60' E; 1363 m a.s.l.), Liang et al. (2009) reported that the cell division in the cambial zone would start within the third week of May and complete by mid-September. A separate study in northwestern China (37°02' N, 104°28' E; 2456 m a.s.l.)

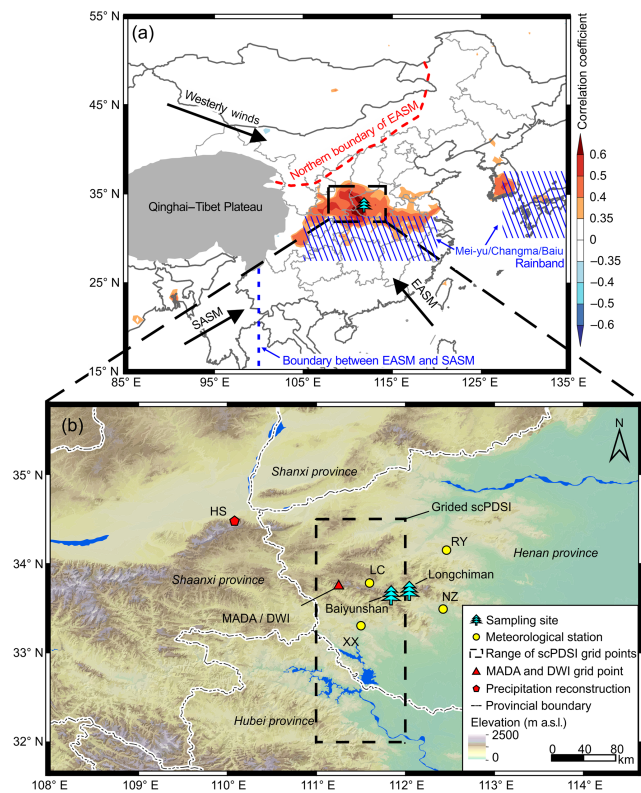


**Figure 1.** Map of the study region. **(a)** Location of the sampling site (tree symbol) and the spatial correlations between the May to July (MJJ) scPDSI reconstruction and the gridded scPDSI dataset (van der Schrier et al., 2013) during the period 1953–2005. The color bar indicates the correlation coefficient. The dashed blue line ( $100^{\circ}$  E) indicates the boundary between East Asian summer monsoon (EASM) and South Asian summer monsoon (SASM; Tang et al., 2010). The dashed red line indicates the northern boundary of EASM (Chen et al., 2018). The blue shaded area represents the Mei-yu/Changma/Baiu rainband (Zhao et al., 2015). **(b)** Partial enlargement of the study region. The circles indicate the locations of the four meteorological stations (LC: Luanchuan, XX: Xixia, RY: Ruyang, and NZ: Nanzhao). The triangle indicates the location of selected grid data from the datasets Monsoon Asia Drought Atlas (MADA; Cook et al., 2010) and Dryness/Wetness Index (DWI; Yang et al., 2013). The pentagon indicates a precipitation reconstruction based on tree-ring width on Mount Hua (HS; Chen et al., 2016b). The dashed rectangle indicates the gridded scPDSI obtained from the gridded scPDSI dataset (van der Schrier et al., 2013).

found that the cambial cells of mature *P. tabuliformis* would start cell division in late spring and cease in late July or early August (Zeng et al., 2018). Since our sampling sites are located at lower latitudes, the cambial activity of *P. tabuliformis* in our study area may start earlier and end later than those found in the abovementioned studies (following the temperature-controlled phenology theory; Chen and Xu, 2012)

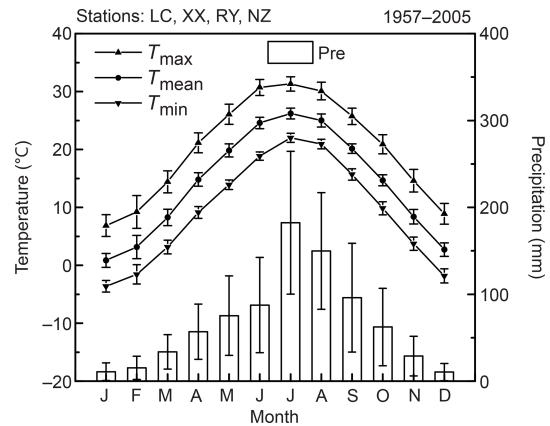


**Figure 2.** Monthly maximum, mean, minimum temperatures ( $T_{\max}$ ,  $T_{\text{mean}}$ ,  $T_{\min}$ ), and total precipitation (Pre) averaged from the four selected meteorological stations (LC: Luanchuan, XX: Xixia, RY: Ruyang, and NZ: Nanzhao) during the period 1957–2005. Error bar denotes  $\pm$  one standard deviation.

*P. tabuliformis* generally exhibits an abrupt transition from light-colored earlywood to dark-colored latewood (Fig. S1 in the Supplement; Liang and Eckstein, 2006). Based on the characteristics of the tree-ring anatomy, the earlywood and latewood segments of annual growth rings can be distinguished visually by the sudden change in cell size, lumen size, and color (Stahle et al., 2009). However, gradual transitions could occur in a few samples, making the earlywood–latewood boundary difficult to differentiate. Therefore, only samples with distinct earlywood and latewood segments were used for subsequent measurements (Knapp et al., 2016). In total, 20 cores from 11 trees and 42 cores from 22 trees were selected from Baiyunshan and Longchiman, respectively. EWW and LWW were then measured using a LINTAB5 system at a resolution of 0.001 mm and TRW was obtained by adding EWW and LWW of the same calendar years together.

### 2.3 Development of tree-ring-width chronologies

Non-climatic growth trends need to be fitted and removed from each “raw” (untreated) EWW, LWW, and TRW series, which is known as detrending (Cook et al., 1990). To check the effects of detrending methods on the preservation of climatic signals, three detrending methods were selected for comparison. These included negative exponential functions combined with linear regression with negative (or zero) slope (NELR), cubic smoothing splines with a 50% frequency cutoff at 67% of the series length (SP67), and age-dependent splines with an initial stiffness of 50 years (SPA50). NELR is a deterministic method based on the assumption that tree radial growth declines monotonically (Cook et al., 1990). SP67 has a good ability to fit the potential low- and middle-frequency perturbations contained in ring-width

series (Cook et al., 1990). It allows no more than half of the amplitude of variations with wavelength of two-thirds of the length of series being preserved in resulting indices (Cook et al., 1990). SPA50 specifies an annually varying 50 % frequency cutoff parameter for each year by adding the initial stiffness with ring age. Comparing with SP67, it makes the resulting spline become more flexible in the early years and progressively stiffer in later years (Melvin et al., 2007). All raw ring-width series were divided by the estimated growth trends, and the resulting detrended ring-width series were averaged to generate the standard (STD) chronologies using the bi-weight robust mean method (Fig. S2). Since the traditionally fitted curves may contain low-frequency climatic signals (known as “trend distortion” problem; Melvin and Briffa, 2008), the signal-free (SSF) method was introduced to create a fitted growth curve without climatic signals by dividing the raw ring-width series by the STD chronology by means of iterations (Melvin and Briffa, 2008). Therefore, we also developed SSF chronologies for climate analysis (Fig. S3). Following the methods described in Osborn et al. (1997), the variance in each chronology was stabilized to minimize the effects of sampling depth. The temporal extension for all width chronologies in Baiyunshan and Longchiman covers the periods 1841–2005 and 1850–2005, respectively. All the above processes were performed using the program RCSsigFree version 45\_v2b (<http://www.ldeo.columbia.edu/tree-ring-laboratory/resources/software>, last access: 21 June 2019; Melvin and Briffa, 2008). Since the number of cores per tree in our study was unequal, the signal of each chronology was estimated using the effective chronology signal ( $R_{\text{bar}_{\text{eff}}}$ ) which incorporates the effective number of cores, within- and between-tree signals (Briffa and Jones, 1990). Besides, the expressed population signal (EPS), a function of  $R_{\text{bar}_{\text{eff}}}$  and the number of trees, was applied to evaluate how well the sample chronology represents the a theoretical chronology (Briffa and Jones, 1990; Wigley et al., 1984). The running  $R_{\text{bar}_{\text{eff}}}$  and EPS for each chronology were calculated over a 51-year window with a 50-year overlap using the function “rwi.stats.running” in R package “dplR” version 1.6.9 (Bunn et al., 2018). The minimum number of common years in any pair of ring-width series required for their correlation was set to 30 (Briffa and Jones, 1990). The reliable period for each chronology was determined based on the widely adopted EPS threshold value of 0.85 (Wigley et al., 1984).

The width chronologies from the two sampling sites show high degrees of coherence as evidenced by their significant positive correlations ( $p < 0.001$ ) during their common period 1850–2005 (Table S1 in the Supplement). Moreover, the positive correlations remain significant ( $p < 0.001$ ) after removing the influence of autocorrelations and linear trends from the tree-ring data (Table S1). These indicate that the two sites share common climatic signals. Therefore, we pooled all raw ring-width series from the two sites and developed composite STD and SSF chronologies for EWW, LWW, and

TRW using the three detrending methods as described above (Fig. S4). Statistics for each chronology including the starting year when  $\text{EPS} \geq 0.85$ , standard deviation, mean sensitivity, and first-order correlation coefficient (AR1) are shown in Table S2. In addition, several statistics were calculated to assess the degree of similarity among the detrended ring-width series over the common period 1915–2005 (Table S3). These statistics are variance explained by the first eigenvector ( $\text{Var}_{\text{pc1}}$ ),  $R_{\text{bar}_{\text{eff}}}$ , signal-to-noise ratio (SNR), and EPS (Briffa and Jones, 1990; Trouet et al., 2006).

## 2.4 Climate data

Monthly mean maximum ( $T_{\text{max}}$ ), minimum ( $T_{\text{min}}$ ), and mean temperature ( $T_{\text{mean}}$ ) and monthly total precipitation (Pre) were gathered from four nearby meteorological stations (Table 1; Fig. 1b). These climate data were obtained from the China Meteorological Administration. Regional temperature values were calculated by averaging the temperature time series from the four stations over their common period 1957–2005. Regional precipitation series were calculated by firstly deriving the regional averages in terms of percentages, then multiplying the regional mean to transform the resulting series back to millimeter units (Jones and Hulme, 1996). The self-calibrated PDSI (scPDSI) and SPEI were also chosen as hydroclimatic factors. Here we used the scPDSI instead of PDSI because it has solved the PDSI problems in spatial comparisons by calculating the duration factors (weighting coefficients for the current moisture anomaly and the previous drought severity) based on the characteristics of the climate at a given location (Wells et al., 2004). The regional scPDSI was calculated by averaging the CRU (Climate Research Unit) scPDSI grids (van der Schrier et al., 2013) over the area between 32 to 34.5° N and 111 to 112° E (Fig. 1b) where the meteorological stations utilized by the CRU dataset were concentrated (Fig. S5; Table S4). The time span of scPDSI was selected as 1953–2005 because the stations used by CRU have a common period starting from July 1952 (Table S4). The SPEI has multi-timescales (Vicente-Serrano et al., 2010). To evaluate the influence of SPEI on monthly, seasonal, and annual timescales, we calculated the regional SPEI on three timescales (1-month, 3-month, and 12-month timescales) using the R package “SPEI” version 1.7 (Beguería and Vicente-Serrano, 2017). The climatic factors used in SPEI calculation were regional  $T_{\text{max}}$ ,  $T_{\text{min}}$ , and Pre, which were derived from the four stations mentioned in Table 1. The time span of SPEI is 1957–2005.

In order to validate the reconstruction, we compared it with several hydroclimate time series and historical document records (Table 2). They were (1) the June–August PDSI from the no. 370 grid point of the Monsoon Asia Drought Atlas (MADA) at 33.75° N, 111.25° E over the period 1868–2005 ( $\text{PDSI}_{\text{Cook}}$ ; Cook et al., 2010); (2) the Dryness/Wetness Index (DWI) from the grid point at 33.75° N,

**Table 1.** Characteristics of climate data series used in correlation analyses.

Climate data	Source	Longitude (° E)	Latitude (° N)	Elevation (m a.s.l.)	Temporal cover
$T_{\max}$ , $T_{\text{mean}}$ , $T_{\min}$ , Pre	Luanchuan (LC) meteorological station	111.6	33.8	750.3	1957–2005
	Xixia (XX) meteorological station	111.5	33.3	250.3	1957–2005
	Ruyang (RY) meteorological station	112.5	34.2	307.8	1957–2005
	Nanzhao (NZ) meteorological station	112.6	33.6	199.7	1956–2005
scPDSI	CRU scPDSI 3.25 (van der Schrier et al., 2013)	111–112	32–34.5	–	1953–2005
SPEI	Calculated in R using the SPEI package with the monthly maximum and minimum temperature, and total precipitation (Beguería and Vicente-Serrano, 2017)	–	–	–	1957–2005

111.25° E over the period 1868–2000 (DWI<sub>Yang</sub>; Yang et al., 2013); (3) reconstructed April–June precipitation based on TRW on Mount Hua over the period 1868–2005 (Pre<sub>Chen</sub>; Chen et al., 2016b); and (4) drought or wet events recorded in historical documents over the period 1868–2005 (He, 1980; Wen, 2006). The DWI dataset was reconstructed from the historical documents and modern instrumental May–September precipitation in 120 sites over China (Chinese Academy of Meteorological Sciences, 1981). The dataset classified the degree of dryness and wetness into five grades: very wet (grade 1), wet (grade 2), normal (grade 3), dry (grade 4), and very dry (grade 5). Yang et al. (2013) has interpolated the DWI dataset into 2.5° latitude and longitude grid cells.

The EASM circulation was represented using the newly defined EASMI based on the 200 hPa zonal wind anomalies, which was less affected by complex weather processes near the surface (Zhao et al., 2015). It was computed using

$$\begin{aligned} \text{EASMI} = & \text{Nor} [u(2.5\text{--}10^\circ \text{N}, 105\text{--}140^\circ \text{E}) \\ & - u(17.5\text{--}22.5^\circ \text{N}, 105\text{--}140^\circ \text{E}) \\ & + u(30\text{--}37.5^\circ \text{N}, 105\text{--}140^\circ \text{E})], \end{aligned} \quad (1)$$

where Nor and  $u$  are standardization and mean 200 hPa zonal wind, respectively. To understand the possible impacts of local precipitation and temperature (32–34.5° N and 111–112° E) on the relationship between the scPDSI and EASMI, the precipitation and temperature data were extracted from the gridded precipitation dataset Global Precipitation Climatology Centre Version 7 (GPCC v7; Schneider et al., 2015) and gridded temperature dataset Climatic Research Unit Time-Series Version 4.01 (CRU TS 4.01; Harris et al., 2014), respectively. The gridded dataset can represent the variations in precipitation and temperature over East China in the 20th century (Wang and Wang, 2017; Wen et al., 2006).

## 2.5 Statistical methods

To investigate the climate response of different tree-ring parameters (EWW, LWW, and TRW), we first calculated the Pearson correlation coefficients of the STD and SSF tree-ring-width chronologies using monthly climate time series. The time window for the correlation analysis spanned from January of 2 years earlier before tree-ring formation to October of the current growth year. Next, correlations were calculated between the prewhitened and linearly detrended chronologies and climate time series in order to evaluate the possible effects of autocorrelations and secular trends. The prewhitening procedure was performed using the “ar” function in R package “stats” version 3.5.1 (R Core Team, 2018). The appropriate autoregressive order was automatically determined by the Akaike information criterion (Akaike, 1974). The linear detrending procedure was performed based on the “detrend” function in MATLAB R2016a (MathWorks Inc., 2016). To find the strongest climate–growth relationship, we analyzed the response of different tree-ring parameters to multi-month averaged scPDSI (which had the stronger impacts on tree growth than other climatic factors; see the results for details). Finally, we adopted the wavelet coherence method (Grinsted et al., 2004) to test the temporal stability and possible lags of the climate–growth relationship on different frequency domains.

A simple linear regression model was applied to establish the transfer function using May–July (MJJ) scPDSI as the predictand and the NELR-based EWW STD chronology as the predictor (which had the strongest relationship; see the “Results and discussion” section for details) over the period 1953–2005. Temporal stability of the model was tested by splitting the MJJ scPDSI into two subperiods (1953–1979 and 1979–2005) for calibration and verification. In the process, some statistics (including correlation coefficient ( $r$ ), explained variance ( $R^2$ ), reduction of error (RE), coefficient of efficiency (CE) and the sign test) were applied (Meko and Graybill, 1995). Meanwhile, the possible autocorrelation and trend contained in the regression residuals were evalu-

**Table 2.** Long-term hydroclimatic reconstructions and East Asian summer monsoon index (EASMI) selected for comparing with the reconstructed MJJ scPDSI from this study.

Time series	Source	Longitude (° E)	Latitude (° N)	Temporal cover
June–August PDSI	Monsoon Asia Drought Atlas (MADA; Cook et al., 2010)	111.25	33.75	1868–2005
April–June precipitation on Mount Hua (HS)	Chen et al. (2016b)	110.08	34.47	1868–2005
Dryness/Wetness Index (DWI)	Yang et al. (2013)	111.25	33.75	1868–2000
EASMI	Calculated using the 200 hPa zonal wind anomalies (NOAA-20C; Compo et al., 2011) according to the definition of Zhao et al. (2015)	–	–	1868–2005

ated using the Durbin–Watson test (DW; Durbin and Watson, 1950) using the “dwtest” function in R package “Lmtest” version 0.9-36 (Zeileis and Hothorn, 2002), and the two-sided Cox and Stuart trend test (CS; Cox and Stuart, 1955) using the R package “snpar” version 1.0 (Qiu, 2014), respectively. A DW value of 2 means no first-order autocorrelation in the residuals, whereas values larger (less) than 2 indicate negative (positive) autocorrelation. The DW test has the null hypothesis that the autocorrelation of the residuals is 0. The two-sided CS trend test has the null hypothesis that there is no monotonic trend in the residuals. The variance in the MJJ scPDSI reconstruction was adjusted to match the variance in instrumental MJJ scPDSI during the calibration period using Eq. (2),

$$\text{Adj\_Rec}_i = \frac{\text{Rec}_i - \overline{\text{Rec}_{\text{cal}}}}{\sigma(\text{Rec}_{\text{cal}})} \times \sigma(\text{Ins}_{\text{cal}}) + \overline{\text{Ins}_{\text{cal}}}, \quad (2)$$

where the  $\text{Rec}_i$  and  $\text{Adj\_Rec}_i$  are the reconstructed value and its variance adjusted value for a specific year  $i$ , respectively. The  $\overline{\text{Rec}_{\text{cal}}}$  and  $\overline{\text{Ins}_{\text{cal}}}$  are the arithmetic mean of the reconstructed and instrumental values during the calibration period (it is 1953–2005 in this study), respectively. The  $\sigma(\text{Rec}_{\text{cal}})$  and  $\sigma(\text{Ins}_{\text{cal}})$  are the corresponding standard deviations.

To evaluate the spatial representativeness of our reconstruction, spatial correlations were calculated between the reconstructed MJJ scPDSI and CRU scPDSI 3.25 dataset (van der Schrier et al., 2013) using the KNMI Climate Explorer (<http://climexp.knmi.nl/start.cgi>, last access: 21 June 2019). For comparison purposes, all the hydroclimatic reconstructions were divided into interannual (< 10 years) and decadal and longer-term components (> 10 years). Decadal and longer-frequency components were derived by low-pass filtering of the original reconstructions using the adaptive 10-point Butterworth low-pass filter at 0.1 cutoff frequency (Mann, 2008). Interannual frequency components were obtained by subtracting the decadal and longer-term components from the original reconstructions. The low-

pass filtering technique is capable of preserving trends near time series boundaries (Mann, 2008).

Following the definition of Zhao et al. (2015), we calculated the MJJ EASMI using the 200 hPa zonal wind dataset. The data covering the period 1868–2005 were obtained from the National Oceanic and Atmospheric Administration and Cooperative Institute for Research in Environmental Sciences 20th Century Reanalysis V2c (NOAA-20C; Compo et al., 2011). The relationship between EASMI and our reconstruction was firstly evaluated using the wavelet coherence method (Grinsted et al., 2004). To explore the connections between precipitation and temperature with scPDSI and EASMI, 21-year moving window correlation analyses were conducted between the decadal-filtered MJJ EASMI, reconstructed scPDSI, local precipitation, and temperature. Moreover, empirical orthogonal function (EOF) analysis and spatial correlation analysis were performed to assess the impacts of the changed leading EASM mode on the relationship between decadal-filtered EASMI and local precipitation. The filtering procedure was conducted using the Butterworth low-pass filter (Mann, 2008) as mentioned above. The filtering, EOF, and correlation analyses were performed in MATLAB R2016a (MathWorks Inc., 2016) and the plots were drawn with Surfer 10 (Golden Software, LLC, 2011).

The significance tests for all observed correlation coefficients were conducted using the Monte Carlo method (Efron and Tibshirani, 1986). In detail, modeled time series with the same structure as the original series were produced in accordance to the frequency domain method of Ebisuzaki (1997). Then, correlation coefficients were computed between the modeled time series. The above processes were repeated 1000 times to obtain 1000 modeled correlation coefficients. The significance threshold was estimated based on the probability distribution of the modeled 1000 correlation coefficients. The procedure was performed using the algorithms of Macias-Fauria et al. (2012).

### 3 Results and discussion

#### 3.1 Stronger hydroclimatic signals derived from EWW

The EWW chronologies generated using different detrending and standardization methods were significantly negatively correlated with  $T_{\max}$  and  $T_{\text{mean}}$  during May–June, and significantly positively correlated with precipitation in May (Fig. 3). By relating to drought indices, all EWW chronologies were significantly positively correlated with the 1-month SPEI in May; 3-month SPEI during May–June; 12-month SPEI during May–October; and scPDSI during April–October. Particularly, EWW showed a much longer-term response to the multi-month SPEI and scPDSI than to precipitation after May. This may be because the summer temperatures affected the soil water status as reflected by their negative correlations with EWW. Besides, soil has a memory effect for previous drought conditions, and this effect is considered in the multi-month SPEI and scPDSI (Dai, 2011; Vicente-Serrano et al., 2010). The scPDSI had higher correlation with tree-ring width than the SPEI. This indicates that the scPDSI is more suitable for monitoring the influence of soil moisture status on tree growth at our sampling sites; however, the reasons for this remain unknown at the moment. The significant correlations between EWW and drought indices during autumn should not be regarded as a real drought impact, as the earlywood growth would terminate in the mid- and late-growing seasons (Larson, 1969). For LWW, during the current growing season, the highest correlation was found between the NELR-based LWW STD and July scPDSI ( $r = 0.37$ ,  $p < 0.01$ ). However, this correlation was much lower than that between the NELR-based EWW STD and the July scPDSI ( $r = 0.62$ ,  $p < 0.01$ ), indicating that LWW was less sensitive to the scPDSI. TRW generally exhibited a similar climate response as EWW but with relatively lower correlations. Taking the NELR-based STD chronologies as an example, the correlation coefficients between TRW and the monthly scPDSI from May to July were 0.59 ( $p < 0.01$ ), 0.58 ( $p < 0.01$ ), and 0.58 ( $p < 0.01$ ), respectively. However, for EWW, these correlation coefficients were 0.66 ( $p < 0.01$ ), 0.66 ( $p < 0.01$ ), and 0.62 ( $p < 0.01$ ), respectively. Similar response patterns were also revealed by the correlation coefficients between the prewhitened and linearly detrended series (Fig. 4), indicating that autocorrelations and secular trends in the tree-ring-width chronologies and climate time series had limited effects on the relationships with climate.

Significant climate–growth relationships were also observed in months prior to the current growing season. For example, most of EWW and LWW chronologies exhibited negative response to  $T_{\max}$  and  $T_{\text{mean}}$  during the late summer and early autumn of the previous year (Figs. 3 and 4). High temperatures in the late-growing season of previous year may enhance soil water evaporation, thus inducing moisture stress and limiting the accumulation of photosynthetic products

available for the next year's tree growth (Peng et al., 2014). The influence of moisture status prior to the current growing season is also reflected by the significant positive correlations between LWW and drought indices from September of 2 years earlier to May of the previous year. However, EWW had lower correlations with these monthly drought indices. A plausible explanation may be that the interannual variations in EWW were mainly contributed by the moisture status of the growth year.

Since the impacts of scPDSI on tree growth can last for several months, we analyzed the responses of various tree-ring-width parameters to the multi-month averaged scPDSI. The strongest climate–growth relationship was found between the NELR-based EWW STD chronology and the MJJ scPDSI ( $r = 0.707$ ;  $p < 0.01$ ; Fig. S6). Meanwhile, correlation coefficients derived from the methods SP67 and SPA50 were 0.67 ( $p < 0.01$ ) and 0.68 ( $p < 0.01$ ), respectively, which were lower than those based on the NELR method (Fig. S6). This may be because the downward trend in MJJ scPDSI was better preserved using the NELR detrending method (Fig. S7). In addition, the correlation coefficient between the NELR-based EWW SSF chronology and the MJJ scPDSI was 0.705 ( $p < 0.01$ ), which was quite close to that using the traditional STD method, indicating that the effects of so-called “trend distortion” in our tree-ring series were small.

We further tested the temporal stability and possible lags (leads) in the relationships between NELR-based STD chronologies and the MJJ scPDSI on different frequency domains (Fig. 5). EWW generally has high degrees of coherence with the MJJ scPDSI on all timescales (2- to 18-year timescales), except for the periodicities between 3.5- and 6.5-year. By contrast, LWW only varied in-phase with the MJJ scPDSI, but with some lags during the period from the 1970s to the 1990s on the timescales shorter than 12 years. Moreover, LWW was inversely correlated with the MJJ scPDSI during the 1960s in the 4- to 6-year periodicities. TRW showed an unstable relationship and certain lags to the MJJ scPDSI in the 6- to 11-year periodicities. Therefore, it can be concluded that EWW has more stable relationships with the MJJ scPDSI than LWW and TRW.

Previous studies based on TRW demonstrated that moisture status of the current growing season could strongly affect the radial growth of *P. tabuliformis* (e.g., Cai and Liu, 2013; Cai et al., 2014, 2015; Chen et al., 2014; Fang et al., 2010a, 2012b; Li et al., 2007; Liang et al., 2007; Liu et al., 2017; Song and Liu, 2011; Sun et al., 2012). Fast radial growth of *P. tabuliformis* usually occurs during the early-growing season (Liang et al., 2009; Shi et al., 2008; Zeng et al., 2018). Increased water deficiency due to the rising temperature and inadequate rainfall in the early-growing season induces water stress, suppressing cell division and expansion (Fritts, 1976), and resulting in the formation of narrow earlywood bands. The reduced sensitivity of LWW to moisture status of the current growing season may be due to that ample wa-

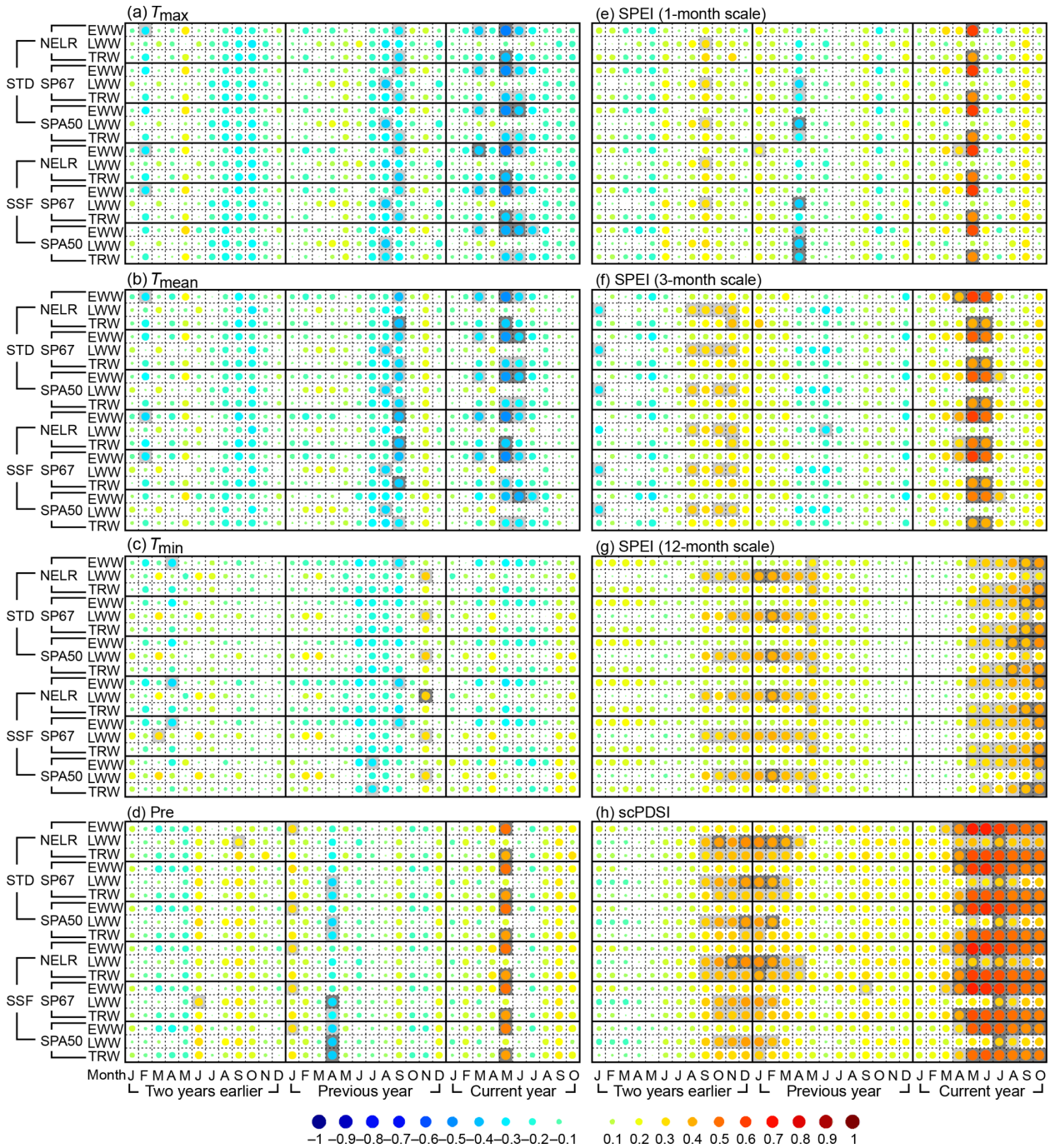


**Figure 3.** Matrix plots for the correlation coefficients between tree-ring-width chronologies and monthly climate time series from January of 2 years earlier to October of the current year. The climatic factors are monthly (a) maximum temperature ( $T_{max}$ ), (b) mean temperature ( $T_{mean}$ ), (c) minimum temperature ( $T_{min}$ ), (d) total precipitation (Pre), (e) SPEI of 1-month scale, (f) SPEI of 3-month scale, (g) SPEI of 12-month scale, and (h) scPDSI. The EWW, LWW, and TRW represent the earlywood width, latewood width, and total tree-ring width, respectively. The correlation analyses were conducted for the period 1953–2005 for the scPDSI and for 1957–2005 for the other climatic factors. NELR, SP67, and SPA50 indicate the three detrending methods: (1) negative exponential functions combined with linear regression with negative (or zero) slope (NELR), (2) cubic smoothing splines with a 50 % frequency cutoff at 67 % of the series length (SP67), and (3) age-dependent splines with an initial stiffness of 50 years (SPA50). STD and SSF indicate the two standardization methods “standard” and “signal-free”, respectively. The correlation coefficients are reflected by the colored and different-size circles, which can be referred to using the color bar as shown at the bottom of the figure. The squares filled with light and dark gray indicate that the correlation coefficients are statistically significant at the 0.05 and 0.01 levels, respectively, which are tested using the Monte Carlo method (Efron and Tibshirani, 1986; Macias-Fauria et al., 2012).

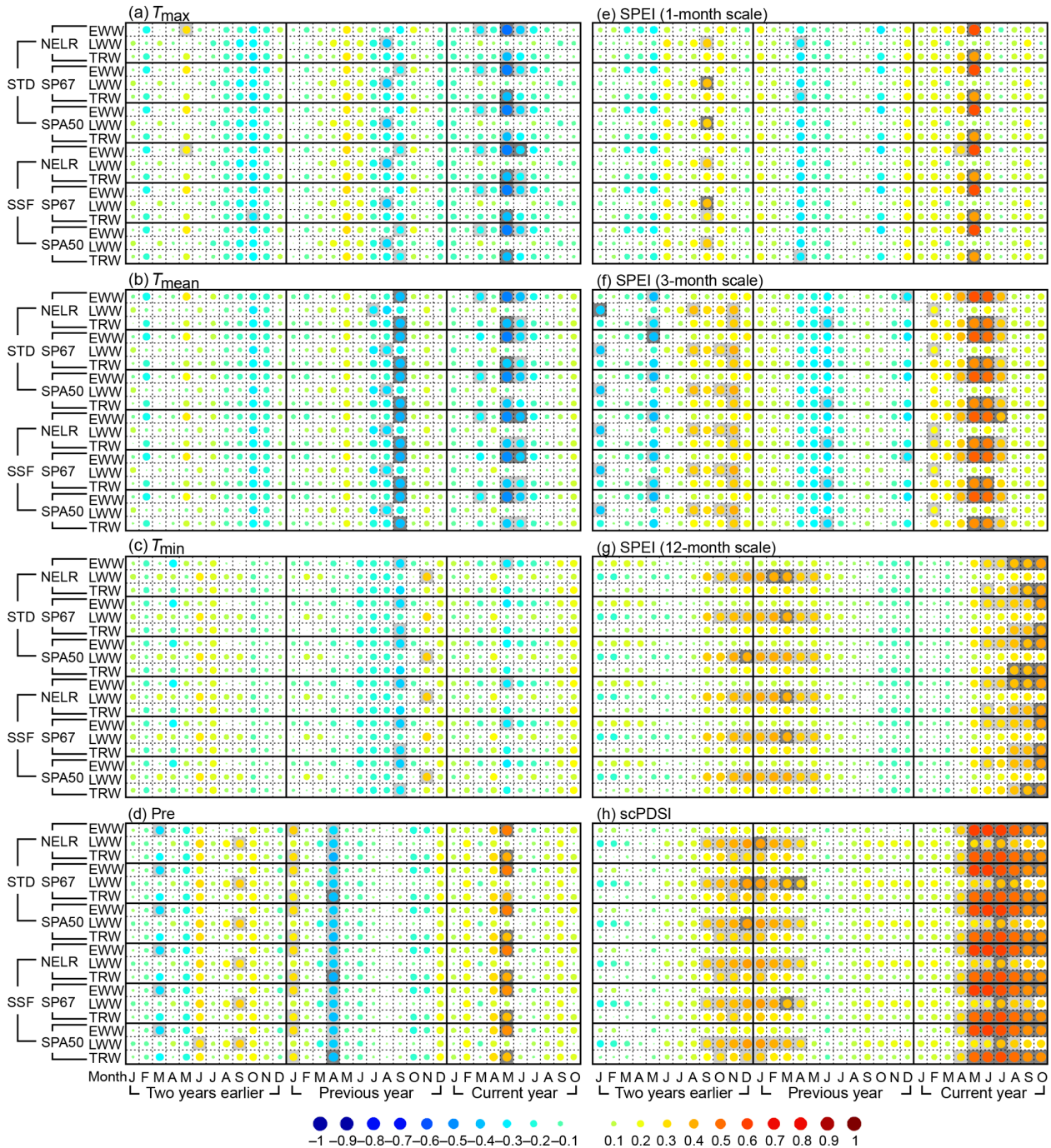


**Figure 4.** Matrix plots for the correlation coefficients between the prewhitened and linearly detrended tree-ring-width chronologies and monthly climate time series from January of 2 years earlier to October of the current year. The climatic factors are monthly (a) maximum temperature ( $T_{max}$ ), (b) mean temperature ( $T_{mean}$ ), (c) minimum temperature ( $T_{min}$ ), (d) total precipitation (Pre), (e) SPEI of 1-month scale, (f) SPEI of 3-month scale, (g) SPEI of 12-month scale, and (h) scPDSI. The EWW, LWW, and TRW represent the earlywood width, latewood width, and total tree-ring width, respectively. The correlation analyses were conducted for the period 1953–2005 for the scPDSI and for 1957–2005 for the other climatic factors. NELR, SP67, and SPA50 indicate the three detrending methods: (1) negative exponential functions combined with linear regression with negative (or zero) slope (NELR), (2) cubic smoothing splines with a 50 % frequency cutoff at 67 % of the series length (SP67), and (3) age-dependent splines with an initial stiffness of 50 years (SPA50). STD and SSF indicate the two standardization methods “standard” and “signal-free”, respectively. The correlation coefficients are reflected by the colored and different-size circles, which can be referred to using the color bar as shown at the bottom of the figure. The squares filled with light and dark gray indicate that the correlation coefficients are statistically significant at the 0.05 and 0.01 levels, respectively, which are tested using the Monte Carlo method (Efron and Tibshirani, 1986; Macias-Fauria et al., 2012).

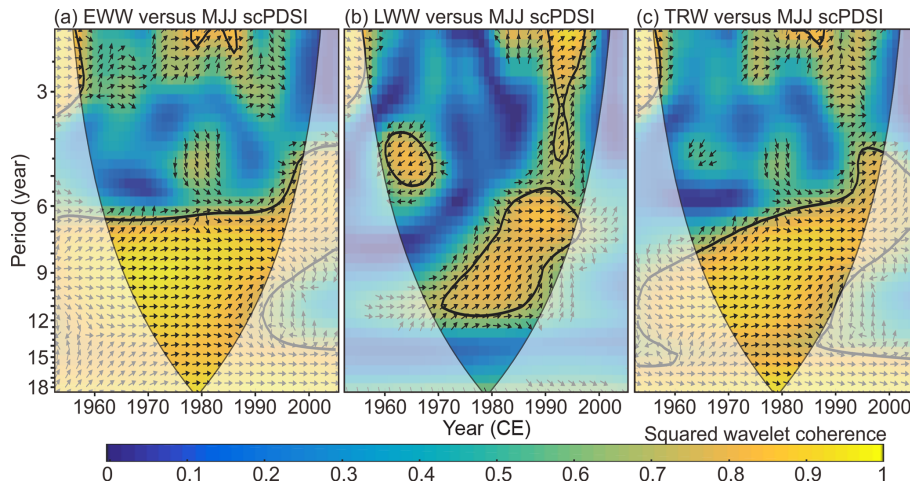


**Figure 5.** Squared wavelet coherence and phase relationship between the NELR-based tree-ring-width STD chronologies and MJJ scPDSI. Panels (a)–(c) represent the results for EWW, LWW, and TRW, respectively. The color bar indicates the squared wavelet coherence. The arrows indicate the phase relationship with in-phase (anti-phase) pointing right (left), and MJJ scPDSI leading (lagging) tree-ring width with  $90^\circ$  pointing straight up (down). The thick contour indicates the 5% significance level against red noise. The cone of influence (COI) where edge effects might distort the picture is marked in a lighter shade.

ter supply in the rainy season (July–August; Fig. 2). TRW and EWW shared similar climatic response. This is because EWW represents the majority of TRW (on average, the portion of EWW of TRW accounts for 65.8%). However, since TRW is also contributed by LWW, the response of TRW to moisture status in the current growing season was somewhat weaker than EWW.

### 3.2 MJJ scPDSI reconstruction using NELR-based EWW STD chronology

From the above analyses, we identified the MJJ scPDSI as the target for hydroclimate reconstruction and the NELR-based EWW STD chronology as the predictor (Fig. 6a). The transfer function was estimated using a simple linear regression model as expressed below:

$$\text{MJJ scPDSI} = 4.74\text{EWW} - 4.32; \quad (3)$$

$$(R^2 = 0.5, n = 53, p < 0.001).$$

The model explained 50% of the actual MJJ scPDSI variance over the period 1953–2005. The calibration–verification tests revealed that  $r$ ,  $R^2$ , and the sign test were significant at the 0.01 level, and that RE and CE values were positive (Table 3). In addition, the  $p$  value generated from DW and CS tests were above 0.05, indicating that there were neither autocorrelation nor long-term trends in the regression residuals (Table 3; Fig. 6b). All test results confirmed that the model is valid (Cook et al., 1999; Fritts, 1976).

Based on Eq. (3), we reconstructed MJJ scPDSI of the study region back to 1868 (Fig. 6c). We adjusted the variance in the reconstruction to match the variance in instrumental MJJ scPDSI during the calibration period (1953–2005).

Spatial correlation analysis indicated that the reconstruction most strongly represents central China, including the western part of Henan, northern part of Hubei, and southern part of Shaanxi provinces (Fig. 1a).

### 3.3 Comparing the reconstructed MJJ scPDSI with other climate reconstructions and historical records

On the interannual timescale (Fig. 7a–c), our reconstruction is significantly correlated with the  $\text{PDSI}_{\text{Cook}}$  ( $r = 0.37$ ;  $p < 0.01$ ; 1868–2005) and  $\text{Pre}_{\text{Chen}}$  ( $r = 0.52$ ;  $p < 0.01$ ; 1868–2005). On the decadal and longer timescales, our reconstruction is significantly correlated with all other reconstructions from the study region (Fig. 7d–f). The common drought periods occurring in the 1870s and the 1920s in northern and western China (Cai et al., 2014; Chen et al., 2014; Fang et al., 2012a; Kang et al., 2013; Liang et al., 2006; Liu et al., 2017; Zhang et al., 2017) were also reflected in our reconstruction.

However, it should be noted that our reconstruction has also some mismatches with others. On the interannual timescale, our reconstruction is not significantly correlated with the  $\text{DWI}_{\text{Yang}}$  over the whole period 1868–2000 ( $r = -0.06$ ;  $p = 0.64$ ; Fig. 7b). This is probably due to the limited ability of historical documents to capture high-frequency climatic variations (Zheng et al., 2014). On the decadal and longer timescales, our reconstruction varied out of phase with  $\text{PDSI}_{\text{Cook}}$  during the period from the late 1940s to the early 1960s (Fig. 7d). It was only weakly correlated with  $\text{DWI}_{\text{Yang}}$  after the 1940s (Fig. 7e) and led  $\text{Pre}_{\text{Chen}}$  during the period of 1900s–1930s (Fig. 7f). This might be due to several reasons. Firstly, the reconstructions focused on different target seasons (June–August for  $\text{PDSI}_{\text{Cook}}$ , May–September for  $\text{DWI}_{\text{Yang}}$ , and April–June for  $\text{Pre}_{\text{Chen}}$ , which is before the

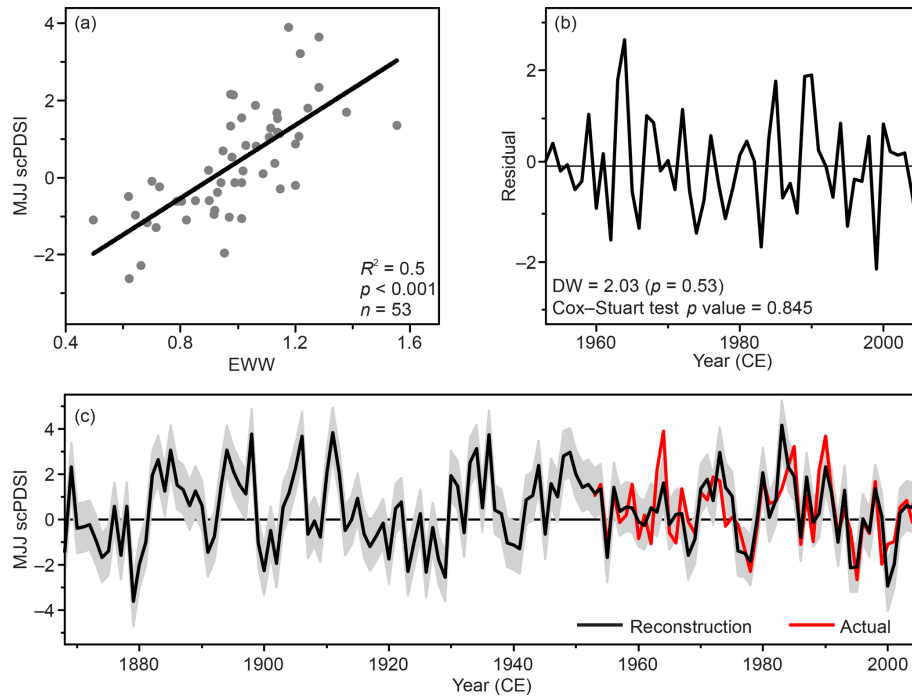


**Figure 6.** MJJ scPDSI reconstruction using NELR-based EWW STD chronology. **(a)** Scatter diagram for the period 1953–2005 and **(b)** the resulting residuals. **(c)** MJJ scPDSI reconstruction (black line, after variance adjusted) and instrumental MJJ scPDSI (red line). Shaded area denotes the uncertainties of reconstruction in the form of  $\pm 1$  root-mean-square error.

**Table 3.** Statistics of regression models for split calibration–verification periods.

Calibration period	<i>r</i>	<i>R</i> <sup>2</sup>	DW value ( <i>p</i> value)	CS <i>p</i> value	Verification period	RE	CE	Sign test
Full period (1953–2005)	0.71*	0.50*	2.03 (0.53)	0.85	–	–	–	–
Early half (1953–1979)	0.68*	0.46*	2.02 (0.49)	1	Late half (1979–2005)	0.53	0.53	22 + /5–*
Late half (1979–2005)	0.73*	0.54*	2.02 (0.50)	1	Early half (1953–1979)	0.46	0.45	21 + /6–*

\* *p* < 0.01; *r*, Pearson correlation coefficient; *R*<sup>2</sup>, explained variance; DW, Durbin–Watson test; CS, Cox and Stuart trend test; RE, reduction of error; and CE, coefficient of efficiency.

rainy season). Secondly, the  $DWI_{Yang}$  after the 1940s was calculated using instrumental May–September precipitation and the chronology of Chen et al. (2016b) also reflects precipitation, while the scPDSI is influenced not only by precipitation but also temperature and previous drought conditions. Thirdly, the MADA network includes only a limited number of tree-ring sites in our study region, which may cause deviations on the local scale.

We also compared the dry and wet events derived from our reconstruction with historical records. Following Palmer (1965), the moderately to severely dry (wet) events are defined based on the scPDSI values less than  $-2$  (larger than 2). Interestingly, all dry events and 70 % of the wet events in our reconstruction can be verified by corresponding de-

scriptions in historical records (Table 4). However, there are still some mismatches between our reconstruction and the historical records. For example, no relevant record is found for the year 1983 when an extreme wet event is shown in our reconstruction. Meanwhile, some historical events are not reflected in our reconstruction, such as the wet event in 1963 and the dry event in 1942 (Wen, 2006). In addition, our reconstruction generally demonstrates a wetter condition compared with other series (especially in its early part) and fails to capture the extreme drought years documented in the past (e.g., 1976–1978 and 1914; Wen, 2006). This might be because the low-frequency hydroclimatic variability persevered in EWW was entangled with the declining biological trend, and was partly removed during the detrending process using

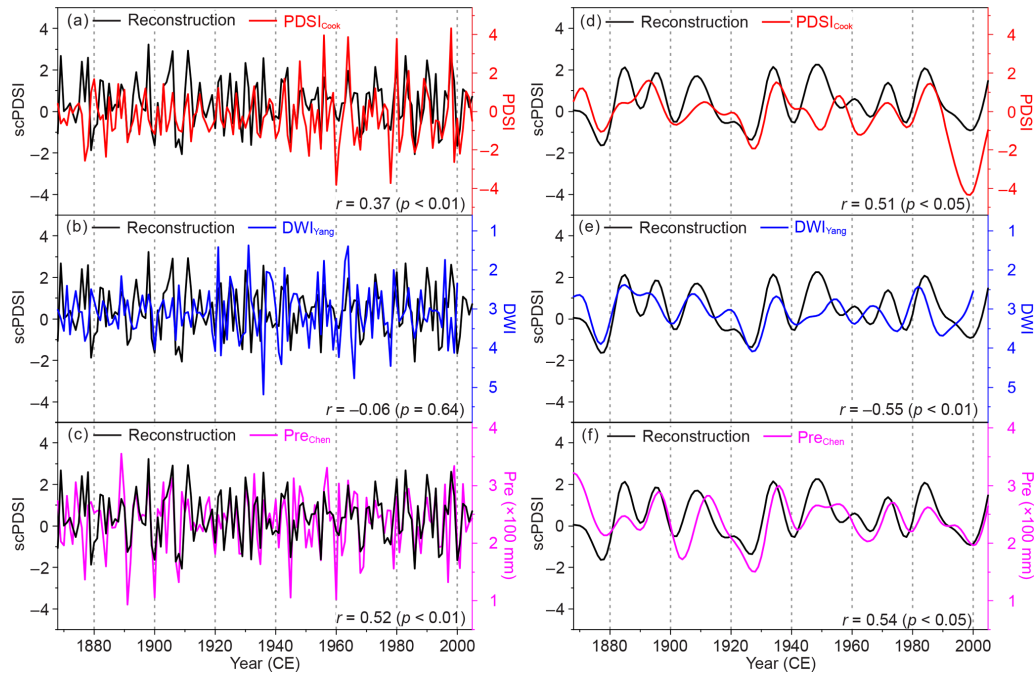


**Figure 7.** Comparison of the reconstructed MJJ scPDSI (black line) with other hydroclimatic reconstructions in adjacent regions on the interannual (**a**, **b**, **c**) and decadal and longer timescales (**d**, **e**, **f**). The referenced reconstructions are (**a**, **d**) June–August PDSI of MADA no. 370 grid point (Cook et al., 2010), (**b**, **e**) reversed DWI (Yang et al., 2013), and (**c**, **f**) TRW-based April–June precipitation (Pre) reconstruction (Chen et al., 2016b). The interannual and decadal and longer fluctuations were separated using the adaptive 10-point Butterworth low-pass filter with 0.1 cutoff frequency (Mann, 2008).  $r$  represents the Pearson correlation coefficient between the reconstructed MJJ scPDSI and other hydroclimatic reconstruction over their common period. The significance level for all correlation coefficients was tested using the Monte Carlo method (Efron and Tibshirani, 1986; Macias-Fauria et al., 2012).

simple curve fitting methods (Briffa et al., 1996). A possible approach to preserving the low-frequency hydroclimatic signals is to adopt the regional curve standardization (RCS) method (Briffa et al., 1992) but this requires more field work in the future to collect additional tree-ring samples with an even distribution of different age classes (Briffa et al., 1996).

### 3.4 Connections with EASMI

In general, the reconstructed MJJ scPDSI and EASMI exhibit an in-phase relationship before the 1940s on the decadal and longer timescales (Fig. 8). This in-phase relationship was further verified after conducting a 21-year moving window correlation analysis on the decadal-filtered scPDSI and EASMI (Fig. 9a, b and e). Since EASM directly drives precipitation rather than the scPDSI, we compared the EASMI with the local precipitation (32 to 34.5° N and 111 to 112° E). We found that the local precipitation also exhibits similar variations as the scPDSI and EASMI before the 1940s (Fig. 9a–c). Therefore, the in-phase relationship between the decadal-filtered EASMI and scPDSI before the 1940s may be due to the fact that a stronger EASM could enhance local precipitation, thus increasing the soil moisture content. Interestingly, the correlation between the local precipitation and EASMI weakened after the 1940s, and even became negative since

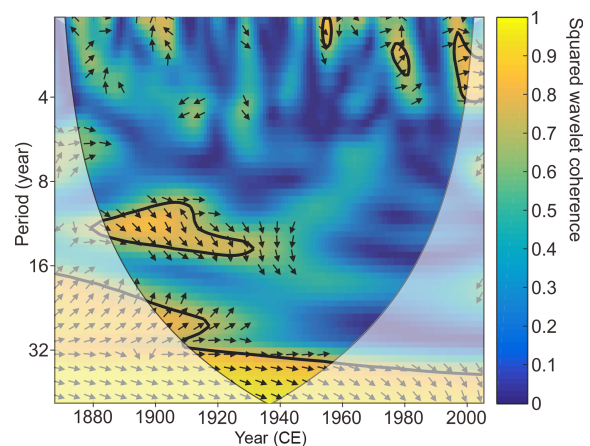


**Figure 8.** Squared wavelet coherence and phase relationship between the reconstructed MJJ scPDSI and EASMI (Zhao et al., 2015). The color bar indicates the squared wavelet coherence. The arrows indicate the phase relationship with in-phase (anti-phase) pointing right (left) and EASMI leading (lagging) scPDSI with 90° pointing straight up (down). The thick contour indicates the 5% significance level against red noise. The cone of influence (COI) where edge effects might distort the picture is marked in a lighter shade.

**Table 4.** Moderately to severely dry ( $\text{scPDSI} \leq -2$ ) and wet ( $\text{scPDSI} \geq 2$ ) events derived from the MJJ scPDSI reconstruction and corresponding descriptions from historical records.

Event type	Year	scPDSI	Description
Dry	1879	-3.61	A mega-drought caused a great famine over Henan, Shaanxi, and other provinces in northern China in the early Guangxu reign (1876–1879)*
	1900	-2.24	Severe drought from spring to autumn over Henan and Shaanxi
	1923	-2.28	Drought over Henan and Shaanxi
	1926	-2.33	No harvest at Ruyang (western Henan) due to severe drought
	1929	-2.53	Summer drought over Henan and Shaanxi
	1994	-2.12	Severe drought occurred in April, May, and July over western Henan
	1995	-2.10	Intensified drought severity since 22 April over Henan
	2000	-2.94	The drought from February to May was the worst one since 1950 over Henan
Wet	1869	2.31	Flood in summer and autumn over Henan
	1883	2.62	Persistent rainfall in summer at Shanxian and Mianchi (northwestern Henan)
	1885	3.07	Flood in summer at Lingbao and Shanxian (northwestern Henan)
	1894	3.06	Not available
	1895	2.11	Flood of the Qinhe River (northwestern Henan) in summer
	1898	3.77	Severe flood in summer at Lushi (northwestern Henan), Shangnan (southeast Shaanxi), and Danjiang (northwestern Hubei)
	1905	2.26	Persistent rainfall in spring and summer over Henan
	1906	3.65	Heavy rainfall in summer over Henan
	1910	2.05	Flood in summer and autumn over Henan
	1911	3.84	Heavy rainfall in summer over Henan
	1912	2.01	Heavy rainfall and flood in summer over Nanyang (southwestern Henan)
	1933	2.51	Heavy rainfall in summer over Henan and Shaanxi
	1934	3.11	Summer rainfall over Henan, southern Shaanxi, and northwestern Hubei
	1936	3.72	Not available
	1944	2.38	Flood over Henan; rainstorm in Zhenan (southeastern Shaanxi) on 8 July; the Tianhui Channel (southeast Shaanxi) was destroyed by flood on 13 May
	1948	2.81	Wheat loss caused by summer rainfall
	1949	2.95	Not available
	1973	2.97	Not available
	1980	2.07	Rainfall in June was higher than usual for most regions over Henan
	1983	4.15	Not available
1984	2.33	From June to September, there were 5 large-scale rainstorms over Henan	
1900	2.32	Not available	

\* Historical description of the 1879 drought event is cited from He (1980), and others from Wen (2006).

the 1970s (Fig. 9e). We attribute this unstable relationship to the variable nature of EASMI. In fact, the EASMI was designed to capture the leading mode of EASM precipitation variability, whose largest loading is in general located at the Mei-yu/Changma/Baiu rainband (Zhao et al., 2015). In other words, the Mei-yu/Changma/Baiu rainfall has the most robust relationship with the EASMI. Whilst the leading pattern of EASM precipitation could change on inter-decadal and longer timescales (which is still elusive due to the limited paleoprecipitation record), the unique importance of Mei-yu/Changma/Baiu in EASM most likely remains (Wang et al., 2008). With the changing precipitation pattern of EASM, the precipitation outside of the Mei-yu/Changma/Baiu rainband could be in phase, out of phase, and uncorrelated with Mei-yu/Changma/Baiu rainfall (Wang

et al., 2008), which would manifest an unstable relationship with EASMI. The EASM experienced an abrupt shift in the late 1970s, which caused a change in the leading mode of EASM precipitation (Ding et al., 2008; Wang, 2001). We demonstrated how this mode change affects the relationship between EASMI and precipitation in the eastern Qinling Mountains. As shown in Fig. 10a, the anomalies of the decadal-filtered MJJ precipitation exhibited similar variations over the Yangtze River basin and Yellow–Huaihe river basins during 1901–1978. However, they were divided by the Yangtze River, showing a dipole pattern during 1979–2005 (Fig. 10b). During both periods, the loading centers were located south of the Yangtze River basin (27–30° N), and the decadal-filtered MJJ precipitation in this area was captured well by the designed EASMI as manifested by their signifi-

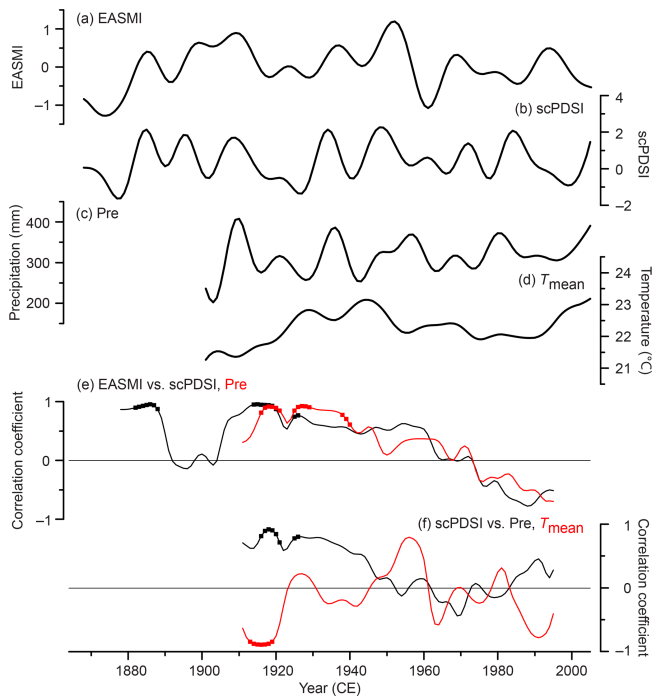


**Figure 9.** Comparison between the decadal and longer fluctuations of May–July (a) EASMI (Zhao et al., 2015), (b) reconstructed scPDSI, (c) precipitation (Pre; GPCP v7; Schneider et al., 2015), and (d) mean temperature ( $T_{\text{mean}}$ ; CRU TS 4.01; Harris et al., 2014) over the area of reconstruction. (e) The 21-year moving Pearson correlation coefficients of the decadal-filtered EASMI with scPDSI (black), and Pre (red). (f) The 21-year moving Pearson correlations of the decadal filtered scPDSI with Pre (black), and  $T_{\text{mean}}$  (red). The decadal and longer fluctuations were derived using the adaptive 10-point Butterworth low-pass filter with 0.1 cutoff frequency (Mann, 2008). Statistically significant ( $p < 0.05$ ) correlations are denoted as squares, which were tested using the Monte Carlo method (Efron and Tibshirani, 1986; Macias-Fauria et al., 2012).

icant positive correlations ( $p < 0.1$ ; Fig. 10c and d). On the contrary, the decadal-filtered MJJ precipitation north of the Yangtze River (including our sampling sites) varied out of phase with that south of the Yangtze River basin after the late 1970s, thus being negatively correlated with the EASMI.

The weakened scPDSI–EASMI relationship after the 1940s cannot be solely attributed to the change in the EASM precipitation mode because the scPDSI showed a weakened relationship with the local precipitation simultaneously (Fig. 10f). Neither can it be ascribed simply by the fact that the variations in scPDSI became dominated by temperature either as no enhanced scPDSI–temperature relationship was found (Fig. 10f). This may be because the scPDSI is not a simple formula based on precipitation and temperature, but a complex function incorporating previous drought conditions and current moisture departure (Wells et al., 2004). In addition to the precipitation and temperature, the available energy, humidity, and wind speed can also affect the scPDSI via

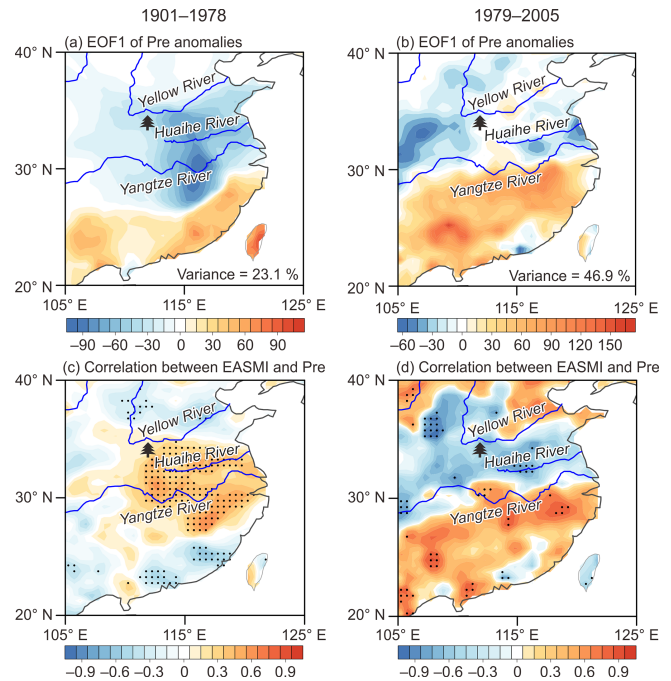


**Figure 10.** (a–b) The leading empirical orthogonal function (EOF) modes of decadal filtered May–July GPCP precipitation anomalies for the periods 1901–1978 (a) and 1979–2005 (b). The color bar indicates the EOF values. (c–d) Spatial correlations between the decadal filtered May–July EASMI defined by Zhao et al. (2015) and precipitation (Pre) for the periods 1901–1978 (c) and 1979–2005 (d). The color bar indicates the correlation coefficient. Dots indicate correlation significant at  $p < 0.1$ . Decadal-scale and longer-term fluctuations of precipitation were derived using the adaptive 10-point Butterworth low-pass filter with 0.1 cutoff frequency (Mann, 2008). The tree symbol denotes the study region.

controlling evapotranspiration (Sheffield et al., 2012). Therefore, a variety of climate data are required to identify the specific cause for the observed weakened relationship. However, an exact determination of the causing factors is difficult due to the limited existing climate records.

## 4 Conclusions

Besides TRW, climatic responses of EWW and LWW were also explored for the tree-ring samples of *P. tabuliformis* from the eastern Qinling Mountains, central China. Regardless of the detrending and standardization methods used, the resulting EWW chronologies are more sensitive to early summer soil moisture conditions (scPDSI) than LWW and TRW during the instrumental period 1953–2005. The MJJ scPDSI (1868–2005) reconstructed from the NELR-based EWW STD chronology captures the past early summer hydroclimatic fluctuations, which is further validated by other proxy-based reconstructions and historical document records from adjacent regions. This indicates that EWW has a great potential to reconstruct early summer hydroclimatic con-

ditions in the study area. Moreover, on the decadal and longer timescales, our EWW-based hydroclimate reconstruction shows a strong in-phase relationship with the EASMI before the 1940s, which may be related to the positive response of the local precipitation to EASM intensity. Our finding differs from results developed at a well-drained site in southern China, where strongest moisture signals are contained in LWV of a different tree species (Zhao et al., 2017a, b). Therefore, more EWW- and LWV-related studies should be conducted to reveal the tree- and site-specific climate signals in humid and semi-humid regions of China.

**Data availability.** The reconstructed May–July scPDSI is included in the Supplement (Table S5). DWI, precipitation reconstruction, and dry or wet events recorded in historical documents are available from corresponding authors or publications. MADA is available from <https://www.ncdc.noaa.gov/paleo-search/study/10435> (last access: 21 June 2019, Cook et al., 2010). The 200 hPa zonal wind dataset of NOAA-20C is available from [https://www.esrl.noaa.gov/psd/data/gridded/data.20thC\\_ReanV2c.html](https://www.esrl.noaa.gov/psd/data/gridded/data.20thC_ReanV2c.html) (last access: 21 June 2019, Compo et al., 2011). The gridded dataset CRU scPDSI 3.25 is available from <https://crudata.uea.ac.uk/cru/data/drought/> (last access: 21 June 2019, van der Schrier et al., 2013). The gridded precipitation dataset GPCC v7 is available from [https://opendata.dwd.de/climate\\_environment/GPCC/html/fulldata\\_v7\\_doi\\_download.html](https://opendata.dwd.de/climate_environment/GPCC/html/fulldata_v7_doi_download.html) (last access: 21 June 2019, Schneider et al., 2015). The gridded temperature dataset CRU TS 4.01 is available from [https://crudata.uea.ac.uk/cru/data/hrg/cru\\_ts\\_4.01/cruts.1709081022.v4.01/tmp/](https://crudata.uea.ac.uk/cru/data/hrg/cru_ts_4.01/cruts.1709081022.v4.01/tmp/) (last access: 21 June 2019, Harris et al., 2014).

**Supplement.** The supplement related to this article is available online at: <https://doi.org/10.5194/cp-15-1113-2019-supplement>.

**Author contributions.** YZ and JS designed the study. JS provided the tree-ring samples. YZ performed tree-ring-width measurement, data analyses, and interpretation. JS, SS, XS, and HL assisted in data interpretation. YZ wrote the first draft of the paper. All authors revised the paper.

**Competing interests.** The authors declare that they have no conflict of interest.

**Acknowledgements.** We thank Feng Chen for providing his reconstructed precipitation data, and Zhou Yu for his help in tree-ring-width measurements. We would also like to express our gratitude to EditSprings (<https://www.editsprings.com/>, last access: 21 June 2019) for the expert linguistic services provided.

**Financial support.** This research has been supported by the Key R&D Program of China (grant no. 2016YFA0600503), the Na-

tional Natural Science Foundation of China (grant no. 41671193), the China Scholarship Council (grant nos. 201706190150 and 201806195033).

**Review statement.** This paper was edited by Hans Linderholm and reviewed by two anonymous referees.

## References

- Akaike, H.: A new look at the statistical model identification, *IEEE T. Automat. Contr.*, 19, 716–723, <https://doi.org/10.1109/TAC.1974.1100705>, 1974.
- Beguéría, S. and Vicente-Serrano, S. M.: SPEI: Calculation of the Standardised Precipitation-Evapotranspiration Index, available at: <https://CRAN.R-project.org/package=SPEI> (last access: 21 June 2019), r package version 1.7, 2017.
- Briffa, K. R. and Jones, P. D.: Basic chronology statistics and assessment, in: *Methods of Dendrochronology: Applications in the Environmental Sciences*, edited by: Cook, E. R. and Kairiukstis, L. A., 137–152, Kluwer Academic Publishers, Dordrecht, the Netherlands, <https://doi.org/10.1007/978-94-015-7879-0>, 1990.
- Briffa, K. R., Jones, P. D., Bartholin, T. S., Eckstein, D., Schweingruber, F. H., Karlén, W., Zetterberg, P., and Eronen, M.: Fennoscandian summers from AD 500: temperature changes on short and long timescales, *Clim. Dynam.*, 7, 111–119, <https://doi.org/10.1007/BF00211153>, 1992.
- Briffa, K. R., Jones, P. D., Schweingruber, F. H., Karlén, W., and Shiyatov, S. G.: Tree-ring variables as proxy-climate indicators: problems with low-frequency signals, in: *Climatic variations and forcing mechanisms of the last 2000 years*, edited by: Jones, P. D., Bradley, R. S., and Jouzel, J., 9–41, Springer, Berlin, Heidelberg, [https://doi.org/10.1007/978-3-642-61113-1\\_2](https://doi.org/10.1007/978-3-642-61113-1_2), 1996.
- Bunn, A., Korpela, M., Biondi, F., Campelo, F., Mérian, P., Qeadan, F., Zang, C., Pucha-Cofrep, D., and Wernicke, J.: dplR: Dendrochronology Program Library in R, available at: <https://CRAN.R-project.org/package=dplR> (last access: 21 June 2019), r package version 1.6.9, 2018.
- Cai, Q. and Liu, Y.: Climatic response of Chinese pine and PDSI variability in the middle Taihang Mountains, north China since 1873, *Trees*, 27, 419–427, <https://doi.org/10.1007/s00468-012-0812-6>, 2013.
- Cai, Q., Liu, Y., Lei, Y., Bao, G., and Sun, B.: Reconstruction of the March–August PDSI since 1703 AD based on tree rings of Chinese pine (*Pinus tabulaeformis* Carr.) in the Lingkong Mountain, southeast Chinese loess Plateau, *Clim. Past*, 10, 509–521, <https://doi.org/10.5194/cp-10-509-2014>, 2014.
- Cai, Q., Liu, Y., Liu, H., and Ren, J.: Reconstruction of drought variability in North China and its association with sea surface temperature in the joining area of Asia and Indian–Pacific Ocean, *Palaeogeogr. Palaeoclimatol.*, 417, 554–560, <https://doi.org/10.1016/j.palaeo.2014.10.021>, 2015.
- Cai, Q., Liu, Y., Liu, H., Sun, C., and Wang, Y.: Growing-season precipitation since 1872 in the coastal area of subtropical southeast China reconstructed from tree rings and its relationship with the East Asian summer monsoon system, *Ecol. Indic.*, 82, 441–450, <https://doi.org/10.1016/j.ecolind.2017.07.012>, 2017.

- Chen, F., Yuan, Y., Wen, W., Yu, S., Fan, Z., Zhang, R., Zhang, T., and Shang, H.: Tree-ring-based reconstruction of precipitation in the Changling Mountains, China, since A.D.1691, *Int. J. Biometeorol.*, 56, 765–774, <https://doi.org/10.1007/s00484-011-0431-8>, 2012.
- Chen, F., Yuan, Y., Zhang, R., and Qin, L.: A tree-ring based drought reconstruction (AD 1760–2010) for the Loess Plateau and its possible driving mechanisms, *Global Planet. Change*, 122, 82–88, <https://doi.org/10.1016/j.gloplacha.2014.08.008>, 2014.
- Chen, F., Yu, S., Yuan, Y., Wang, H., and Gagen, M.: A tree-ring width based drought reconstruction for southeastern China: links to Pacific Ocean climate variability, *Boreas*, 45, 335–346, <https://doi.org/10.1111/bor.12158>, 2016a.
- Chen, F., Zhang, R., Wang, H., Qin, L., and Yuan, Y.: Updated precipitation reconstruction (AD 1482–2012) for Huashan, north-central China, *Theor. Appl. Climatol.*, 123, 723–732, <https://doi.org/10.1007/s00704-015-1387-0>, 2016b.
- Chen, J., Huang, W., Jin, L., Chen, J., Chen, S., and Chen, F.: A climatological northern boundary index for the East Asian summer monsoon and its interannual variability, *Sci. China Earth Sci.*, 61, 13–22, <https://doi.org/10.1007/s11430-017-9122-x>, 2018.
- Chen, X. and Xu, L.: Temperature controls on the spatial pattern of tree phenology in China's temperate zone, *Agr. Forest Meteorol.*, 154–155, 195–202, <https://doi.org/10.1016/j.agrformet.2011.11.006>, 2012.
- Chinese Academy of Meteorological Sciences: Yearly charts of dryness/wetness in China for the last 500-year period, China Cartographic Publishing House, Beijing, China, 1981 (in Chinese).
- Compo, G. P., Whitaker, J. S., Sardeshmukh, P. D., Matsui, N., Allan, R. J., Yin, X., Gleason, B. E., Vose, R. S., Rutledge, G., Bessemoulin, P., Brönnimann, S., Brunet, M., Crouthamel, R. I., Grant, A. N., Groisman, P. Y., Jones, P. D., Kruk, M. C., Kruger, A. C., Marshall, G. J., Mauerer, M., Mok, H. Y., Nordli, Ø., Ross, T. F., Trigo, R. M., Wang, X. L., Woodruff, S. D., and Worley, S. J.: The twentieth century reanalysis project, *Q. J. Roy. Meteorol. Soc.*, 137, 1–28, <https://doi.org/10.1002/qj.776>, 2011.
- Cook, E. R., Briffa, K. R., Shiyatov, S. G., and Mazepa, V.: Tree-ring standardization and growth-trend estimation, in: *Methods of Dendrochronology: Applications in the Environmental Sciences*, edited by: Cook, E. R. and Kairiukstis, L. A., 104–123, Kluwer Academic Publishers, Dordrecht, Netherlands, <https://doi.org/10.1007/978-94-015-7879-0>, 1990.
- Cook, E. R., Meko, D. M., Stahle, D. W., and Cleaveland, M. K.: Drought reconstructions for the continental United States, *J. Climate*, 12, 1145–1162, [https://doi.org/10.1175/1520-0442\(1999\)012<1145:DRFTCU>2.0.CO;2](https://doi.org/10.1175/1520-0442(1999)012<1145:DRFTCU>2.0.CO;2), 1999.
- Cook, E. R., Anchukaitis, K. J., Buckley, B. M., D'Arrigo, R. D., Jacoby, G. C., and Wright, W. E.: Asian monsoon failure and megadrought during the last millennium, *Science*, 328, 486–489, <https://doi.org/10.1126/science.1185188>, 2010.
- Cox, D. R. and Stuart, A.: Some quick sign tests for trend in location and dispersion, *Biometrika*, 42, 80–95, <https://doi.org/10.2307/2333424>, 1955.
- Dai, A.: Characteristics and trends in various forms of the Palmer Drought Severity Index during 1900–2008, *J. Geophys. Res.*, 116, D12115, <https://doi.org/10.1029/2010JD015541>, 2011.
- Ding, Y., Wang, Z., and Sun, Y.: Inter-decadal variation of the summer precipitation in East China and its association with decreasing Asian summer monsoon. Part I: Observed evidences, *Int. J. Climatol.*, 28, 1139–1161, <https://doi.org/10.1002/joc.1615>, 2008.
- Ding, Y., Sun, Y., Liu, Y., Si, D., Wang, Z., Zhu, Y., Liu, Y., Song, Y., and Zhang, J.: Interdecadal and interannual variabilities of the Asian summer monsoon and its projection of future change, *Chinese J. Atmos. Sci.*, 37, 253–280, <https://doi.org/10.3878/j.issn.1006-9895.2012.12302>, 2013 (in Chinese).
- Durbin, J. and Watson, G. S.: Testing for serial correlation in least squares regression: I, *Biometrika*, 37, 409–428, <https://doi.org/10.2307/2332391>, 1950.
- Ebisuzaki, W.: A method to estimate the statistical significance of a correlation when the data are serially correlated, *J. Climate*, 10, 2147–2153, [https://doi.org/10.1175/1520-0442\(1997\)010<2147:AMTETS>2.0.CO;2](https://doi.org/10.1175/1520-0442(1997)010<2147:AMTETS>2.0.CO;2), 1997.
- Efron, B. and Tibshirani, R.: Bootstrap methods for standard errors, confidence intervals, and other measures of statistical accuracy, *Stat. Sci.*, 1, 54–75, 1986.
- Fan, Z.-X., Bräuning, A., and Cao, K.-F.: Tree-ring based drought reconstruction in the central Hengduan Mountains region (China) since A.D. 1655, *Int. J. Climatol.*, 28, 1879–1887, <https://doi.org/10.1002/joc.1689>, 2008.
- Fang, K., Gou, X., Chen, F., D'Arrigo, R., and Li, J.: Tree-ring based drought reconstruction for the Guiqing Mountain (China): linkages to the Indian and Pacific Oceans, *Int. J. Climatol.*, 30, 1137–1145, <https://doi.org/10.1002/joc.1974>, 2010a.
- Fang, K., Gou, X., Chen, F., Li, J., D'Arrigo, R., Cook, E., Yang, T., and Davi, N.: Reconstructed droughts for the southeastern Tibetan Plateau over the past 568 years and its linkages to the Pacific and Atlantic Ocean climate variability, *Clim. Dynam.*, 35, 577–585, <https://doi.org/10.1007/s00382-009-0636-2>, 2010b.
- Fang, K., Gou, X., Chen, F., Frank, D., Liu, C., Li, J., and Kazmer, M.: Precipitation variability during the past 400 years in the Xiaolong Mountain (central China) inferred from tree rings, *Clim. Dynam.*, 39, 1697–1707, <https://doi.org/10.1007/s00382-012-1371-7>, 2012a.
- Fang, K., Gou, X., Chen, F., Liu, C., Davi, N., Li, J., Zhao, Z., and Li, Y.: Tree-ring based reconstruction of drought variability (1615–2009) in the Kongtong Mountain area, northern China, *Global Planet. Change*, 80–81, 190–197, <https://doi.org/10.1016/j.gloplacha.2011.10.009>, 2012b.
- Fritts, H. C.: *Tree rings and climate*, Academic Press, New York, 1976.
- Golden Software, LLC: Surfer version 10.1.561, available at: <https://www.goldensoftware.com/products/surfer> (last access: 21 June 2019), 2011.
- Gou, X., Yang, T., Gao, L., Deng, Y., Yang, M., and Chen, F.: A 457-year reconstruction of precipitation in the southeastern Qinghai-Tibet Plateau, China using tree-ring records, *Chinese Sci. Bull.*, 58, 1107–1114, <https://doi.org/10.1007/s11434-012-5539-7>, 2013.
- Grinsted, A., Moore, J. C., and Jevrejeva, S.: Application of the cross wavelet transform and wavelet coherence to geophysical time series, *Nonlin. Processes Geophys.*, 11, 561–566, <https://doi.org/10.5194/npg-11-561-2004>, 2004.
- Guan, B. T., Wright, W. E., Chiang, L.-H., and Cook, E. R.: A dry season streamflow reconstruction of the critically endangered

- Formosan landlocked salmon habitat, *Dendrochronologia*, 52, 152–161, <https://doi.org/10.1016/j.dendro.2018.10.008>, 2018.
- Hansen, K. G., Buckley, B. M., Zottoli, B., D'Arrigo, R. D., Nam, L. C., Truong V. V., Nguyen, D. T., and Nguyen, H. X.: Discrete seasonal hydroclimate reconstructions over northern Vietnam for the past three and a half centuries, *Climatic Change*, 145, 177–188, <https://doi.org/10.1007/s10584-017-2084-z>, 2017.
- Harris, I., Jones, P. D., Osborn, T. J., and Lister, D. H.: Updated high-resolution grids of monthly climatic observations – the CRU TS3.10 Dataset, *Int. J. Climatol.*, 34, 623–642, <https://doi.org/10.1002/joc.3711>, 2014.
- He, H. W.: *Guangxu chunian (1876–1879) Huabei de dahanzai (The North China drought famine of the early Guangxu reign (1876–1879))*, Chinese University of Hong Kong Press, Hong Kong, 1980 (in Chinese).
- Hughes, M. K., Wu, X., Shao, X., and Garfin, G. M.: A preliminary reconstruction of rainfall in north-central China since A.D. 1600 from tree-ring density and width, *Quaternary Res.*, 42, 88–99, <https://doi.org/10.1006/qres.1994.1056>, 1994.
- Jiang, Z., He, J., Li, J., Yang, J., and Wang, J.: Northerly advancement characteristics of the East Asian summer monsoon with its interdecadal variations, *Acta Geographica Sinica*, 61, 675–686, <https://doi.org/10.11821/xb200607001>, 2006 (in Chinese).
- Jones, P. D. and Hulme, M.: Calculating regional climatic time series for temperature and precipitation: methods and illustrations, *Int. J. Climatol.*, 16, 361–377, [https://doi.org/10.1002/\(SICI\)1097-0088\(199604\)16:4<361::AID-JOC53>3.0.CO;2-F](https://doi.org/10.1002/(SICI)1097-0088(199604)16:4<361::AID-JOC53>3.0.CO;2-F), 1996.
- Kang, S., Yang, B., Qin, C., Wang, J., Shi, F., and Liu, J.: Extreme drought events in the years 1877–1878, and 1928, in the southeast Qilian Mountains and the air–sea coupling system, *Quaternary Int.*, 283, 85–92, <https://doi.org/10.1016/j.quaint.2012.03.011>, 2013.
- Knapp, P. A., Maxwell, J. T., and Soulé, P. T.: Tropical cyclone rainfall variability in coastal North Carolina derived from longleaf pine (*Pinus palustris* Mill.): AD 1771–2014, *Climatic Change*, 135, 311–323, <https://doi.org/10.1007/s10584-015-1560-6>, 2016.
- Larson, P. R.: *Wood formation and the concept of wood quality*, Bulletin no. 74, 1–54, New Haven, CT: Yale University, School of Forestry, 1969.
- Lei, Y., Liu, Y., Song, H., and Sun, B.: A wetness index derived from tree-rings in the Mt. Yishan area of China since 1755 AD and its agricultural implications, *Chinese Sci. Bull.*, 59, 3449–3456, <https://doi.org/10.1007/s11434-014-0410-7>, 2014.
- Li, J., Chen, F., Cook, E. R., Gou, X., and Zhang, Y.: Drought reconstruction for north central China from tree rings: the value of the Palmer drought severity index, *Int. J. Climatol.*, 27, 903–909, <https://doi.org/10.1002/joc.1450>, 2007.
- Li, J., Shi, J., Zhang, D. D., Yang, B., Fang, K., and Yue, P. H.: Moisture increase in response to high-altitude warming evidenced by tree-rings on the southeastern Tibetan Plateau, *Clim. Dynam.*, 48, 649–660, <https://doi.org/10.1007/s00382-016-3101-z>, 2017.
- Li, Y., Fang, K., Cao, C., Li, D., Zhou, F., Dong, Z., Zhang, Y., and Gan, Z.: A tree-ring chronology spanning 210 years in the coastal area of southeastern China, and its relationship with climate change, *Clim. Res.*, 67, 209–220, <https://doi.org/10.3354/cr01376>, 2016.
- Liang, E. and Eckstein, D.: Light rings in Chinese pine (*Pinus tabulaeformis*) in semiarid areas of north China and their palaeo-climatological potential, *New Phytol.*, 171, 783–791, <https://doi.org/10.1111/j.1469-8137.2006.01775.x>, 2006.
- Liang, E., Liu, X., Yuan, Y., Qin, N., Fang, X., Huang, L., Zhu, H., Wang, L., and Shao, X.: The 1920s drought recorded by tree rings and historical documents in the semi-arid and arid areas of northern China, *Climatic Change*, 79, 403–432, <https://doi.org/10.1007/s10584-006-9082-x>, 2006.
- Liang, E., Shao, X., Liu, H., and Eckstein, D.: Tree-ring based PDSI reconstruction since AD 1842 in the Ortindag Sand Land, east Inner Mongolia, *Chinese Sci. Bull.*, 52, 2715–2721, <https://doi.org/10.1007/s11434-007-0351-5>, 2007.
- Liang, E., Eckstein, D., and Shao, X.: Seasonal cambial activity of relict Chinese pine at the northern limit of its natural distribution in North China—Exploratory results, *IAWA J.*, 30, 371–378, <https://doi.org/10.1163/22941932-90000225>, 2009.
- Liu, H., Shao, X., and Huang, L.: Reconstruction of early-summer drought indices in mid-north region of China after 1500 using tree ring chronologies, *Quaternary Sciences*, 22, 220–229, 2002 (in Chinese).
- Liu, X., Nie, Y., and Wen, F.: Seasonal dynamics of stem radial increment of *Pinus taiwanensis* Hayata and its response to environmental factors in the Lushan Mountains, Southeastern China, *Forests*, 9, 387, <https://doi.org/10.3390/f9070387>, 2018.
- Liu, Y., Zhang, X., Song, H., Cai, Q., Li, Q., Zhao, B., Liu, H., and Mei, R.: Tree-ring-width-based PDSI reconstruction for central Inner Mongolia, China over the past 333 years, *Clim. Dynam.*, 48, 867–879, <https://doi.org/10.1007/s00382-016-3115-6>, 2017.
- Liu, Y., Song, H., Sun, C., Song, Y., Cai, Q., Liu, R., Lei, Y., and Li, Q.: The 600-mm precipitation isoline distinguishes tree-ring-width responses to climate in China, *Natl. Sci. Rev.*, 6, 359–368, <https://doi.org/10.1093/nsr/nwy101>, 2018.
- Macias-Fauria, M., Grinsted, A., Helama, S., and Holopainen, J.: Persistence matters: Estimation of the statistical significance of paleoclimatic reconstruction statistics from autocorrelated time series, *Dendrochronologia*, 30, 179–187, <https://doi.org/10.1016/j.dendro.2011.08.003>, 2012.
- Mann, M. E.: Smoothing of climate time series revisited, *Geophys. Res. Lett.*, 35, L16708, <https://doi.org/10.1029/2008gl034716>, 2008.
- MathWorks Inc.: MATLAB and Statistics Toolbox Release 2016a, available at: <https://www.mathworks.com> (last access: 21 June 2019), 2016.
- Meko, D. and Graybill, D. A.: Tree-ring reconstruction of upper Gila River discharge, *Water Resour. Bull.*, 31, 605–616, <https://doi.org/10.1111/j.1752-1688.1995.tb03388.x>, 1995.
- Melvin, T. M. and Briffa, K. R.: A “signal-free” approach to dendroclimatic standardisation, *Dendrochronologia*, 26, 71–86, <https://doi.org/10.1016/j.dendro.2007.12.001>, 2008.
- Melvin, T. M., Briffa, K. R., Nicolussi, K., and Grabner, M.: Time-varying-response smoothing, *Dendrochronologia*, 25, 65–69, <https://doi.org/10.1016/j.dendro.2007.01.004>, 2007.
- Osborn, T. J., Biffa, K. R., and Jones, P. D.: Adjusting variance for sample-size in tree-ring chronologies and other regional mean timeseries, *Dendrochronologia*, 15, 89–99, 1997.
- Palmer, W. C.: *Meteorological drought*, Research paper No. 45, 1–58, US Weather Bureau, Washington DC, 1965.

- Peng, J., Liu, Y., and Wang, T.: A tree-ring record of 1920's–1940's droughts and mechanism analyses in Henan Province, *Acta Ecologica Sinica*, 34, 3509–3518, <https://doi.org/10.5846/stxb201306121687>, 2014 (in Chinese).
- Qiu, D.: snpar: Supplementary Non-parametric Statistics Methods, available at: <https://CRAN.R-project.org/package=snpar> (last access: 21 June 2019), r package version 1.0, 2014.
- R Core Team: R: A Language and Environment for Statistical Computing, R Foundation for Statistical Computing, Vienna, Austria, available at: <https://www.R-project.org/> (last access: 21 June 2019), 2018.
- Schneider, U., Becker, A., Finger, P., Meyer-Christoffer, A., Rudolf, B., and Ziese, M.: GPCC full data monthly product version 7.0 at 0.5°: Monthly land-surface precipitation from rain-gauges built on GTS-based and historic data, Global Precipitation Climatology Centre (GPCC), Berlin, Germany, [https://doi.org/10.5676/DWD\\_GPCC/FD\\_M\\_V7\\_050](https://doi.org/10.5676/DWD_GPCC/FD_M_V7_050), 2015.
- Sheffield, J., Wood, E. F., and Roderick, M. L.: Little change in global drought over the past 60 years, *Nature*, 491, 435–438, <https://doi.org/10.1038/nature11575>, 2012.
- Shi, J., Liu, Y., Vaganov, E. A., Li, J., and Cai, Q.: Statistical and process-based modeling analyses of tree growth response to climate in semi-arid area of north central China: A case study of *Pinus tabulaeformis*, *J. Geophys. Res.*, 113, G01026, <https://doi.org/10.1029/2007JG000547>, 2008.
- Shi, J., Li, J., Cook, E. R., Zhang, X., and Lu, H.: Growth response of *Pinus tabulaeformis* to climate along an elevation gradient in the eastern Qinling Mountains, central China, *Clim. Res.*, 53, 157–167, <https://doi.org/10.3354/cr01098>, 2012.
- Shi, J., Lu, H., Li, J., Shi, S., Wu, S., Hou, X., and Li, L.: Tree-ring based February–April precipitation reconstruction for the lower reaches of the Yangtze River, southeastern China, *Global Planet. Change*, 131, 82–88, <https://doi.org/10.1016/j.gloplacha.2015.05.006>, 2015.
- Song, H. and Liu, Y.: PDSI variations at Kongtong Mountain, China, inferred from a 283-year *Pinus tabulaeformis* ring width chronology, *J. Geophys. Res.-Atmos.*, 116, D22111, <https://doi.org/10.1029/2011jd016220>, 2011.
- Stahle, D. W., Cleaveland, M. K., Grissino-Mayer, H. D., Griffin, R. D., Fye, F. K., Therrell, M. D., Burnette, D. J., Meko, D. M., and Villanueva Diaz, J.: Cool and warm-season precipitation reconstructions over western New Mexico, *J. Climate*, 22, 3729–3750, <https://doi.org/10.1175/2008JCLI2752.1>, 2009.
- Sun, J., Liu, Y., Sun, B., and Wang, R.: Tree-ring based PDSI reconstruction since 1853 AD in the source of the Fenhe River Basin, Shanxi Province, China, *Sci. China Earth Sci.*, 55, 1847–1854, <https://doi.org/10.1007/s11430-012-4369-4>, 2012.
- Tang, X., Chen, B., Liang, P., and Qian, W.: Definition and features of the north edge of the East Asian summer monsoon, *J. Meteorol. Res.-PRC*, 24, 43–49, 2010.
- Trouet, V., Coppin, P., and Beeckman, H.: Annual growth ring patterns in *Brachystegia spiciformis* reveal influence of precipitation on tree growth, *Biotropica*, 38, 375–382, <https://doi.org/10.1111/j.1744-7429.2006.00155.x>, 2006.
- van der Schrier, G., Barichivich, J., Briffa, K. R., and Jones, P. D.: A scPDSI-based global data set of dry and wet spells for 1901–2009, *J. Geophys. Res.-Atmos.*, 118, 4025–4048, <https://doi.org/10.1002/jgrd.50355>, 2013.
- Vicente-Serrano, S. M., Beguería, S., and López-Moreno, J. I.: A multiscalar drought index sensitive to global warming: the standardized precipitation evapotranspiration index, *J. Climate*, 23, 1696–1718, <https://doi.org/10.1175/2009JCLI2909.1>, 2010.
- Wang, B., Wu, Z., Li, J., Liu, J., Chang, C.-P., Ding, Y., and Wu, G.: How to measure the strength of the East Asian summer monsoon, *J. Climate*, 21, 4449–4463, <https://doi.org/10.1175/2008jcli2183.1>, 2008.
- Wang, D. and Wang, A.: Applicability assessment of GPCP and CRU precipitation products in China during 1901 to 2013, *Climatic and Environmental Research*, 22, 446–462, <https://doi.org/10.3878/j.issn.1006-9585.2016.16122>, 2017 (in Chinese).
- Wang, H.: The weakening of the Asian monsoon circulation after the end of 1970's, *Adv. Atmos. Sci.*, 18, 376–386, <https://doi.org/10.1007/BF02919316>, 2001.
- Wang, L., Fang, K., Chen, D., Dong, Z., Zhou, F., Li, Y., Zhang, P., Ou, T., Guo, G., Cao, X., and Yu, M.: Intensified variability of the El Niño–Southern Oscillation enhances its modulations on tree growths in southeastern China over the past 218 years, *Int. J. Climatol.*, 38, 5293–5304, <https://doi.org/10.1002/joc.5730>, 2018.
- Wells, N., Goddard, S., and Hayes, M. J.: A self-calibrating Palmer drought severity index, *J. Climate*, 17, 2335–2351, [https://doi.org/10.1175/1520-0442\(2004\)017<2335:ASPSI>2.0.CO;2](https://doi.org/10.1175/1520-0442(2004)017<2335:ASPSI>2.0.CO;2), 2004.
- Wen, K. (Ed.): Meteorological disasters in China, China Meteorological Press, Beijing, China, 2006 (in Chinese).
- Wen, X.-Y., Wang, S.-W., Zhu, J.-H., and David, V.: An overview of China climate change over the 20th century using UK/UEA/CRU high resolution grid data, *Chinese J. Atmos. Sci.*, 30, 894–903, 2006 (in Chinese).
- Wigley, T. M. L., Briffa, K. R., and Jones, P. D.: On the average value of correlated time series, with applications in dendroclimatology and hydrometeorology, *J. Clim. Appl. Meteorol.*, 23, 201–213, [https://doi.org/10.1175/1520-0450\(1984\)023<0201:otavoc>2.0.co;2](https://doi.org/10.1175/1520-0450(1984)023<0201:otavoc>2.0.co;2), 1984.
- Xu, H. C., Sun, Z. F., Guo, G., and Feng, L.: Geographic distribution of *Pinus tabulaeformis* Carr. and classification of provenance regions, *Scientia Silvae Sinicae*, 17, 258–270, 1981 (in Chinese).
- Yang, F., Shi, F., Kang, S., Wang, S., Xiao, Z., Nakatsuka, T., and Shi, J.: Comparison of the dryness/wetness index in China with the Monsoon Asia Drought Atlas, *Theor. Appl. Climatol.*, 114, 553–566, <https://doi.org/10.1007/s00704-013-0858-4>, 2013.
- Zeileis, A. and Hothorn, T.: Diagnostic Checking in Regression Relationships, *R News*, 2, 7–10, available at: <https://CRAN.R-project.org/doc/Rnews/> (last access: 21 June 2019), 2002.
- Zeng, Q., Rossi, S., and Yang, B.: Effects of age and size on xylem phenology in two conifers of Northwestern China, *Front. Plant. Sci.*, 8, 2264, <https://doi.org/10.3389/fpls.2017.02264>, 2018.
- Zhang, Y., Tian, Q., Guillet, S., and Stoffel, M.: 500-yr. precipitation variability in Southern Taihang Mountains, China, and its linkages to ENSO and PDO, *Climatic Change*, 144, 419–432, <https://doi.org/10.1007/s10584-016-1695-0>, 2017.
- Zhang, Y.-B., Zheng, H.-M., Long, R.-Z., and Yang, B.-C.: Seasonal cambial activity and formation of phloem and xylem in eight forest tree species grown in North China, *Scientia Silvae Sinicae*, 18, 366–379, 1982 (in Chinese).
- Zhao, G., Huang, G., Wu, R., Tao, W., Gong, H., Qu, X., and Hu, K.: A new upper-level circulation index for the East

- Asian summer monsoon variability, *J. Climate*, 28, 9977–9996, <https://doi.org/10.1175/jcli-d-15-0272.1>, 2015.
- Zhao, Y., Shi, J., Shi, S., Wang, B., and Yu, J.: Summer climate implications of tree-ring latewood width: A case study of *Tsuga longibracteata* in South China, *Asian Geographer*, 34, 131–146, <https://doi.org/10.1080/10225706.2017.1377623>, 2017a.
- Zhao, Y., Shi, J., Shi, S., Yu, J., and Lu, H.: Tree-ring latewood width based July–August SPEI reconstruction in South China since 1888 and its possible connection with ENSO, *J. Meteorol. Res.-PRC*, 31, 39–48, <https://doi.org/10.1007/s13351-017-6096-4>, 2017b.
- Zheng, J., Ge, Q., Hao, Z., Liu, H., Man, Z., Hou, Y., and Fang, X.: Paleoclimatology proxy recorded in historical documents and method for reconstruction on climate change, *Quaternary Sciences*, 34, 1186–1196, <https://doi.org/10.3969/j.issn.1001-7410.2014.06.07>, 2014 (in Chinese).